BNL-108509-2015-JA

Hydrogenation of CO_2 to Methanol: Importance of Metal-Oxide and Metal-Carbide Interfaces in the Activation of CO_2

José A. Rodriguez*, Ping Liu, Dario J. Stacchiola, Sanjaya Senanayake, Michael G. White and Jingguang G. Chen

Chemistry Department

Brookhaven National Laboratory

Upton, NY 11973, USA

Abstract

The high thermochemical stability of CO_2 makes very difficult the catalytic conversion of the molecule into alcohols or other hydrocarbon compounds which can be used as fuels or the starting point for the generation of fine chemicals. Pure metals and bimetallic systems used for the $CO_2 \rightarrow CH_3OH$ conversion usually bind CO_2 too weakly and, thus, show low catalytic activity. Here, we discuss a series of recent studies that illustrate the advantages of metal-oxide and metal-carbide interfaces when aiming at the conversion of CO_2 into methanol. $CeO_x/Cu(111)$, $Cu/CeO_x/TiO_2(110)$ and $Au/CeO_x/TiO_2(110)$ exhibit an activity for the $CO_2 \rightarrow CH_3OH$ conversion that is 2-3 orders of magnitude higher than that of a benchmark Cu(111) catalyst. In the Cu-ceria and Au-ceria interfaces, the multifunctional combination of metal and oxide centers leads to complementary chemical properties that open active reaction pathways for methanol synthesis. Efficient catalysts are also generated after depositing Cu and Au on TiC(001). In these cases, strong-metal support interactions modify the electronic properties of the admetals and make them active for the binding of CO_2 and its subsequent transformation into CH_3OH at the metal-carbide interfaces.

* Corresponding author, e-mail: rodrigez@bnl.gov, fax: 1-631-344-5815

Keywords: CO_2 activation, CO_2 hydrogenation; methanol synthesis; reverse water-gas shift reaction; metal oxides; metal carbides; copper; gold

I. Introduction

Carbon dioxide (CO_2) is a major air pollutant released into the atmosphere by the combustion of carbonaceous fuels, principally wood, coal, oil derived combustibles and natural gas.[1,2] A rising concentration of CO_2 in the Earth's atmosphere has led to concerns about global climate changes and the possible ocean acidification. In the last decade, the chemistry of CO_2 has received significant attention due to its potential use as an alternative and economical feedstock.[3,4,5] The hydrogenation of CO_2 to alcohols or other hydrocarbon compounds is an important approach for recycling the CO_2 released to the atmosphere in combustion processes.[6] Due to a continuous increase in the industrial demand for methanol, much effort is now being devoted to the conversion of CO_2 to methanol.[7] In principle, the chemical recycling of CO_2 to methanol can provide a renewable, carbon-neutral, source for the production of fuels, a practical way for the storage and transportation of energy, as well as a convenient feedstock for producing olefins such as ethylene and propylene and from them synthetic products of interest in the chemical industry.[2,7,8]

The hydrogenation of CO_2 to methanol and water

$$CO_2 + 3H_2 \rightarrow CH_3OH + H_2O \qquad (1)$$

is an exothermic reaction at room temperature ($\Delta H_{298\,K}$= - 11.8 kcal/mol), but it competes with the methanation reaction ($\Delta H_{298\,K}$= -39.4 kcal/mol)[9]

$$CO_2 + 4H_2 \rightarrow CH_4 + 2H_2O \qquad (2)$$

Thus, a high selectivity towards methanol formation requires the use of catalysts that are able to adsorb and activate CO_2 but do not break both C-O bonds in the molecule. Furthermore, because ΔH and ΔS are both negative in equation (1), the synthesis of

methanol is potentially equilibrium limited a high temperature and ideally one must look for catalyst that operate in an efficient way at temperatures below 450 K.[9, 10] With these constrains in mind, different types of materials have been tested as catalysts for the $CO_2 \rightarrow CH_3OH$ conversion.[2,4,7,11,12,13,14] Most of the catalysts used in the industry involve metal nanoparticles supported on an oxide substrate.[7,10] Cu-based catalysts, which also contain ZnO and/or Al_2O_3 , have been commercially used for more than 50 years.[7,10] They do not cleave both bonds in the molecule, i.e. no methane formation through equation (2), but exhibit poor activity for CO_2 hydrogenation at low temperature ($T < 500$ K).[7,15] An increase in temperature facilitates CO_2 activation, but undesirable CO and H_2O are formed through the reverse water-gas shift reaction (RWGS)

$$CO_2 + H_2 \rightarrow CO + H_2O \qquad (3)$$

As a result, additional H_2 is consumed and methanol production is reduced.[7, 16] Furthermore, the presence of water accelerates the sintering of Cu and ZnO in the catalysts leading to deactivation.[7,17] One can try to improve the performance of Cu-based catalysts by making alloys of Cu and a second metal,[4,18,19] but more active and stable catalysts have been obtained recently after depositing copper on novel mixed-metal oxides or on metal carbides.[11,13]

Metal oxides are frequently used as supports for the dispersion of metals and their ability to bind and activate CO_2 largely depends on their basicity and reducibility.[7,20,21,22] Reduced oxides have a strong tendency to react with CO_2.[7,19] By stabilizing the reduced states of an oxide one can enhance its surface chemistry and catalytic activity for CO_2 activation.[11] The stabilization of the reduced states can be achieved by forming oxide-metal or oxide-oxide interfaces.[23,24,25,26,27] For example, experimental and theoretical

studies for the CeO_x/Cu and CeO_x/TiO_2 systems have shown that at small coverages of ceria, the ceria nanoparticles favor a +3 oxidation state.[28,29,30,31] Furthermore, in an oxide-metal interface, in addition to the changes in the reducibility of the oxide, one can also observe a perturbation in the electronic properties of the metal.[32,33,34,35,36] Electronic perturbations can also occur after forming a carbide-metal interface.[37,38,39] In principle, the special synergistic properties associated with oxide-metal and carbide-metal interfaces can be useful for preparing efficient catalysts for CO_2 activation.[11-14,40,41,42,43]

In this Perspective article, we present an overview of recent systematic studies for the conversion of CO_2 to methanol on Cu or Au centers dispersed on oxide and carbide supports. We will start by examining the interaction of CO_2 with extended surfaces and nanoparticles of copper.[4,11,19,44-49] This will allow us to analyze the difficulties associated with the activation of CO_2 and the subsequent $CO_2 \rightarrow CH_3OH$ transformation. Then, we will focus on more complex systems: CO_2 hydrogenation on metal-oxide and metal-carbide interfaces.[11-14] We will pay particular attention to cooperative or synergistic effects involving the metal and the oxide or carbide support. The article ends with a discussion of concepts and approaches that can be useful to design active catalysts for the conversion of CO_2 to methanol and higher alcohols.

II. Transformation of CO_2 to methanol on Cu(111) and Cu nanoparticles

Previous studies have reported fundamental investigations of the hydrogenation of CO_2 on Cu(111), Cu(100) and Cu(110).[4,19,44,45,46,47,48] Experimental and theoretical results indicate that CO_2 interacts weakly with copper surfaces,[4,47,49,50,51] exhibiting a desorption temperature of 100 K.[50] The adsorption of CO_2 is promoted by the presence of adsorbed

atomic O[50] and alkali elements[52] on the copper surface. In general, extended surfaces of copper exhibit a low activity for CO_2 hydrogenation producing mainly CO with methanol as a minority product.[44-47]

Figure 1 shows an Arrhenius plot constructed with steady-state rates for the synthesis of methanol and the RWGS reaction on Cu(111) and on a ZnO(000$\bar{1}$) surface with a Cu coverage of 0.2 ML of Cu.[47] At this Cu coverage, the results of scanning tunneling microscopy (STM) suggest that two- and three-dimensional Cu nanoparticles coexist on the ZnO(000$\bar{1}$) surface.[53] Cu(111) is frequently used as a benchmark for studies of methanol synthesis on copper surfaces.[4,47,51] It is less reactive than the Cu(100) or Cu(110) surfaces.[48-49] The data in Figure 1 shows a significant gain in catalytic activity when going from Cu(111) to nanoparticles of Cu dispersed on ZnO(000$\bar{1}$). The turnover frequency (TOF) for methanol synthesis on Cu(111) at 575 K is 6.3×10^{-3} molecules per Cu site per second.[47] Assuming that all the Cu atoms present in Cu/ZnO(000$\bar{1}$) participate in the reaction, the corresponding TOF for methanol synthesis is 9.3×10^{-2} molecules per Cu site per second. Thus, there is an increase of ~15 times in the rate for the generation of methanol . At the same time a very large enhancement (a factor of ~50) is seen in the rate for the RWGS reaction when going from Cu(111) to Cu/ZnO(000$\bar{1}$). When the data in Figure 1 are compared to results reported in the literature for Cu(110) and polycrystalline copper,[46] one finds the following order of catalytic activity: Cu(111) < polycrystalline copper < Cu(110) < Cu/ZnO(000$\bar{1}$). From the slopes of the lines in the Arrhenius plot of Figure 1 one can calculate apparent activation energies of 25.4 (1.1 eV) and 16.2 kcal/mol (0.7 eV) for the synthesis of methanol on Cu(111) and Cu/ZnO(000$\bar{1}$), respectively. An apparent activation energy of 16 kcal/mol has been

reported for methanol synthesis on Cu(110).[46] In Figure 1, the rate of production of CO through the RWGS is 2-3 orders of magnitude faster than the rate of methanol generation. For example, at a temperature of 575 K, the TOFs for the RWGS on Cu(111) and on Cu/ZnO(000$\bar{1}$) are 1.8 and 86.1 molecules per Cu site per second, respectively. Yet the calculated apparent activation energies for the methanol production and the RWGS were very close[47] suggesting that the two reactions probably share a common key intermediate.

Post-reaction characterization of the Cu(111) and Cu/ZnO(000$\bar{1}$) surfaces using X-ray photoelectron spectroscopy (XPS) showed a strong signal in the C 1s region at binding energies of 289.5–290.0 eV that matched well the position reported for adsorbed formate (HCOO).[47] For the case of Cu(110), post-reaction surface analysis showed that the catalyst was covered by almost a full monolayer of adsorbed HCOO[46] which is probably a fast product of the hydrogenation of CO_2 by H adatoms[4,47,51] as will be discussed below.

Calculations based on density functional theory (DFT) were performed to investigate the $CO_2 \rightarrow CH_3OH$ conversion on Cu(111) and on a Cu_{29} nanoparticle present on the ZnO(000$\bar{1}$) surface.[4,47,51] On the clean copper systems there was no chemisorption of CO_2.[4,47,51] In the experiments of Figure 1, the synthesis of methanol was performed under H_2-rich conditions with H adatoms present on the copper surface. The Cu(111) surface and the Cu_{29} nanoparticle have to be pre-covered with atomic H to facilitate the adsorption of CO_2.[4,47] The reaction with the adsorbed H was highly exothermic (see Figure 2 and ref. 47), producing mainly formate. The formation of a carboxyl species (HOCO) on the copper systems was essentially thermoneutral.[47] Figure 3 displays the calculated energy changes associated with the $CO_2 \rightarrow CH_3OH$ conversion on Cu(111) and on a Cu_{29}

nanoparticle.[47] The presence of corner and edge atoms in the nanoparticle facilitates the chemical transformation but, on both systems, the hydrogenation steps that proceed after the formation of HCOO have large barriers (> 1 eV) making them not efficient. A much more favorable reaction pathway was found for the RWGS reaction,[47] in agreement with the experimental trends seen in Figure 1 and the results reported in refs. 4,44-46.

In order to improve the thermochemistry seen in Figure 3 for the $CO_2 \rightarrow CH_3OH$ conversion, one can follow two different paths. One is to enhance the chemical reactivity of Cu by adding a second metal. This has been done at both experimental and theoretical levels, where some improvement in the thermochemistry and reaction rate for methanol synthesis has been observed.[4,18,19,44,45] Another approach involves the coupling of Cu with and oxide or a carbide substrate.[11,13,43] A comparison of the rates for methanol synthesis on Cu/ZnO($000\bar{1}$)[47] and Cu/TiO_2(110)[11] indicates that the nature of the oxide in contact with copper does matter. On the basis of this, the $CO_2 \rightarrow CH_3OH$ conversion was investigated on a series of catalysts that exhibited different configurations of metal-oxide interfaces.[11,12,54]

III. Transformation of CO_2 to methanol on metal-oxide interfaces

The results in Figure 1 clearly show that Cu/ZnO($000\bar{1}$) works better as a catalyst for the hydrogenation of CO_2 than Cu(111). The deposition of ZnO_x nanoparticles promotes the formation of methanol on Cu(111) and polycrystalline copper.[54] A maximum activity was found for a zinc coverage close to 0.2 ML. At 523 K, the best ZnO_x/Cu system exhibited a turnover frequency (TOF) six times larger than that of plain Cu, see Figure 4, and close to that found for a Cu/ZnO catalyst.[54] Active centers like Cu^{+1}-O-Zn were created in the vicinity of the ZnO_x species.[54] Recent studies of high-resolution transmission

electron microscopy (HRTEM) have detected the formation of a ZnO overlayer on top of the copper particles present in an industrial $Cu/ZnO/Al_2O_3$ catalyst for methanol synthesis.[12] Synergistic effects between Cu and ZnO could be responsible for the catalytic activity of Cu/ZnO.[12,54]

Since CeO_x/Cu(111) has a high catalytic activity for the water-gas shift,[30] its performance in a $CO_2 \rightarrow CH_3OH$ conversion was investigated.[11] The CeO_x/Cu(111) surface was generated by depositing Ce atoms onto a Cu(111) substrate under an atmosphere of O_2.[55] The oxygen reacted with the Cu(111) substrate producing a layer of Cu_2O. On top of this layer, ceria grew as large (20-30 nm) and small particles (< 5 nm), see Figure 5A. The as-prepared surfaces were not stable under the H_2-rich condition used for methanol synthesis. In measurements of ambient pressure X-ray spectroscopy (AP-XPS), the reduction of Cu^{+1} species to Cu^0 and Ce^{4+} to Ce^{3+} was observed.[11] Thus, Ce_2O_3/Cu(111) was the active phase of the catalyst. CeO_x/Cu(111) is a much better catalyst for the production of methanol than either Cu(111), see Figure 5B, or Cu/ZnO(000ī), see Figure 1. In the CeO_x/Cu(111) catalyst, the concentration of active centers at the metal-oxide interface will be at the most equal to the relative area initially covered by the ceria nanoparticles: Or ~ 20% of the concentration of active centers present in a pure Cu(111) substrate. On the basis of this assumption, we estimated a minimum TOF value of 1.3 molecules per active site per second for methanol generation on the CeO_x/Cu(111) catalyst at 575 K. Therefore, the rate for methanol synthesis on CeO_x/Cu(111) is ~ 200 times faster than on Cu(111) and ~ 14 times faster than on Cu/ZnO(000ī). In addition, the apparent activation energy for methanol production is reduced from 25 kcal/mol on plain Cu(111) to 16 kcal/mol on Cu/ZnO(000ī) and 12

kcal/mol on CeO_x/Cu(111).[11]

A combination of ambient-pressure XPS and Infrared Reflection-Absorption Spectroscopy (IRRAS) were used to investigate the interaction of CO_2, H_2 and mixtures of CO_2/H_2 with Cu(111), CeO_2(111) and CeO_x/Cu(111) surfaces at temperatures in the range between 300 and 500 K.[11] In agreement with the results of DFT calculations,[4,47,51] pure CO_2 did not adsorb on Cu(111) at these temperatures . In contrast, the reaction of CO_2 with a CeO_2(111) surface led to the formation of strongly adsorbed carbonate (CO_3^{2-}) species.[11] Exposure of CeO_x/Cu(111) to CO_2 produced carboxylate ($CO_2^{\delta-}$) species on the catalyst surface (Figure 6),[11] indicating that a ceria-copper interface activates CO_2.

Upon annealing the CeOx/Cu(111) system under a mixture of CO_2/H_2 at 500 K, AP-XPS and IRRAS showed the coexistence of $CO_2^{\delta-}$ and formate species on the surface of the catalyst (Figure 6).[11] Only surface formate was detected when a similar experiment was carried out with Cu(111). The carboxylate species were seen in substantial concentrations only when ceria was deposited on the copper substrate. These species were not stable in ultra-high vacuum conditions. The lower stability of $CO_2^{\delta-}$ makes this species a better intermediate for methanol production than bidentate formate species, which have a higher stability and cannot operate as transient species for the $CO_2 \rightarrow CH_3OH$ transformation.[56] Thus, the metal-oxide interface created by the addition of CeO_x nanoparticles to Cu(111) performs well the binding and activation of CO_2, opening a new route for the production of methanol.

DFT calculations were performed to gain insights at a molecular level of the mechanism for methanol synthesis on the CeOx/Cu(111) sample.[11] The surface of the catalyst was modeled using a Ce_6O_{13} cluster supported on a Cu(111) substrate, see Figure

7A. The sequential conversion of CO_2 into methanol occurs under a hydrogen-rich atmosphere. An exothermic hydrogenation of the ceria generates Ce^{3+} cations, which facilitate the binding of CO_2 (ΔE= -12.2 kcal/mol). Over the ceria-copper interface, CO_2 is activated in a bent conformation (Figure 7B). Eventually, the adsorbed CO_2 is hydrogenated yielding a carboxyl OCOH species. The calculated energy barriers for these reaction steps are relatively small (10-11 kcal/mol). An even lower energy barrier of 4.6 kcal/mol is associated with a key OCOH → OC + OH conversion. After this, H_2O is produced from adsorbed H and OH species. Through these steps, the RWGS reaction has occurred . In subsequent steps, sequential hydrogenation of CO to CH_3OH takes place through expected intermediates: Formyl (HCO), formaldehyde (H_2CO), and methoxy (H_3CO).[11] The DFT estimated energy barriers for the sequence of HCO→H_2CO, H_2CO→H_3CO and H_3CO→H_3COH reaction steps are quite small, 5.3, 3.5 and 5 kcal/mol, respectively. Thus, after the first addition of hydrogen to CO, the energy barriers for the following hydrogenation steps are not big (< 6 kcal/mol) and are easily overcome at the temperature (> 450 K) at which the catalytic synthesis of CH_3OH occurs. Under reaction conditions the only intermediates detected in the AP-IR and AP-XPS spectra are $HCOO^-$ (Figure 6 and ref. 11), probably a spectator, and two active species CO_2^- and OH (Figure 6 and ref. 11). The theoretical results show that the energy changes and barriers associated with the synthesis of methanol from CO_2 on a ceria-copper interface are predominantly downhill with an overall exothermic process. This calculated thermochemistry is very different from those calculated for the CO_2 → CH_3OH reaction on pure copper systems (Figure 3) or copper alloys.[4,18,19] In the ceria-copper interface, one have sites of different nature that can work in a cooperative way to facilitate the CO_2 → CH_3OH

transformation.[11]

An analysis of the data in Figure 1 for the Cu(111) and Cu/ZnO(000$\bar{1}$) samples points to an increase in the ability of of copper to catalyze the $CO_2 \rightarrow CH_3OH$ transformation when this element is present in the form of nanoparticles. The same trend is observed in powder systems.[12] Thus, catalysts were prepared by co-depositing nanoparticles of copper and ceria on a TiO_2(110) substrate.[11] On this surface, ceria grows forming small wire-like nanostructures, see Figure 8, in which the Ce^{3+} and Ce^{4+} oxidation states have almost equal stability.[28,29] Images of STM indicate that the ceria nanowires are nucleation centers for the growth of metals such as copper, gold and platinum.[23,28,29] Therefore, the phenomena observed in Figures 5 to 7 for the copper-ceria interface associated with CeO_x/Cu(111) also can take place on the Cu/CeO_x/TiO_2(110) system. In Figure 9, we can see kinetic data for the production of methanol on a catalyst prepared by depositing ~ 0.1 ML of Cu on a TiO_2(110) surface pre-covered 15% by ceria nanoparticles. This system is by far the best catalyst. The supported copper and ceria nanoparticles work in a cooperative way displaying a superior performance with respect to Cu-ZnO interfaces in several configurations.[4,12,47,54] At a temperature of 575 K, a TOF of 8.1 molecules per active site per second has been estimated.[11] On Cu/CeO_x/TiO_2(110) the rate of CH_3OH production is ~ 1280 times faster than on plain Cu(111) and ~ 87 times faster than on a Cu/ZnO(000$\bar{1}$) catalyst. Control experiments for the production of methanol on 0.1 ML of Cu dispersed on TiO_2(110) or CeO_2(111) gave rates that were larger than that of Cu/ZnO(000$\bar{1}$) but substantially lower than the rate of Cu/CeO_x/TiO_2(110) or even CeO_x/Cu(111).[11] Bare CeO_x/TiO_2(110) displayed no activity for the generation of CH_3OH. Therefore, the very high catalytic activity observed for

$Cu/CeO_x/TiO_2(110)$ is likely a consequence of having a metal-oxide interface containing copper and ceria nanoparticles rich in Ce^{3+} sites.[11]

Similar studies have been extended to supported Au catalysts. Bulk metallic gold is chemically inert, but the deposition of gold nanoparticles on $CeO_x/TiO_2(110)$ produces active catalysts for the conversion of CO_2 to methanol.[57] In this aspect, the catalytic activities of $Au/CeO_x/TiO_2(110)$ and $Cu/CeO_x/TiO_2(110)$ are similar, see Figure 10, but the selectivity ratio (rate of methanol synthesis / rate of RWGS) is somewhat better for the gold system.[57] It is remarkable that both catalysts are able to produce methanol under low pressures of 100 mTorr of CO_2 and 700 mTorr of H_2 (T= 573 K). Studies of AP-XPS were carried out under these conditions.[57] In the C 1s region, the $Cu/CeO_x/TiO_2(110)$ and $Au/CeO_x/TiO_2(110)$ surfaces exhibited a clear feature at 289.6 eV. Such feature was not seen on $Cu/TiO_2(110)$ or exhibited a very weak signal on $Au/TiO_2(110)$. It can be assigned to a carboxylate species ($CO_2^{\delta-}$) produced by the decomposition of a HOCO intermediate,[57] which is the product of the reaction of H with CO_2 on the Cu-ceria and Au-ceria interfaces.

Figure 11 displays energy changes calculated for the $CO_2 \rightarrow CH_3OH$ conversion on metal-oxide interfaces created by depositing a Au_3 cluster on clean $TiO_2(110)$ and on a $Ce_2O_x/TiO_2(110)$ surface.[57] The charge transfer between Au_3 and the $TiO_2(110)$ substrate was found to be essentially zero. On the other hand, when the Au_3 cluster was in contact with the $CeO_x/TiO_2(110)$ surface, see Figure 12, there was a substantial charge redistribution, with Au atoms becoming negatively charged. This redistribution of electrons facilitated the adsorption of CO_2 on the surface. The DFT calculations predicted adsorption of the molecule with its positively charge C atom on a $Au^{\delta-}$ site and a negatively charged O atom on a Ce^{3+} site.[57] An analysis of the structures associated with

the reaction energetics in Figure 11 indicates that the $CO_2 \rightarrow CH_3OH$ conversion occurs at the Au-ceria or Au-titania interfaces.[57] The conversion occurs in sequential steps with the RWGS reaction taking place first followed by the hydrogenation of the produced CO to methanol. Large energy barriers are observed for the hydrogenation of CO_2 to HOCO and for the hydrogenation of CO to HCO. The first hydrogenation is the rate determining step. The performance of the Au-ceria interface makes $Au_3/CeO_x/TiO_2(110)$ a better catalyst for methanol synthesis than $Au_3/TiO_2(110)$ or Cu(111) (Figure 3). It is important to stress that in $Cu/CeO_x/TiO_2$ and $Au/CeO_x/TiO_2$ one needs ceria nanoparticles rich in Ce^{3+} centers. These Ce^{3+} centers are essential for the binding and conversion of CO_2.[11,57] Once the ceria particles become relatively big in size, Ce^{4+} is a preferred oxidation state, and the Cu-ceria and Au-ceria interfaces then display catalytic activities close to those found for copper-zinc ozide interfaces present in Cu/ZnO catalysts frequently used for the synthesis of methanol.[4,12,47,54]

In summary, the results described above indicate that the proper choice of a metal-oxide interface can produce active catalysts for the production of CH_3OH from CO_2. The metal and the oxide can participate both in the activation of CO_2 and electronic perturbations produced by the formation of a metal-oxide interface can lead to synergistic catalytic properties.

IV. Transformation of CO_2 to methanol on metal-carbide interfaces

In the last three decades, it has become clear that metal carbides can be useful supports for the dispersion of metals.[13,37-41,43,58] The metal carbides display interesting catalytic properties on their own[39,59,60,61] and they also can change the reactivity of a

supported metal through chemical bonding.[37,62] Studies of CO_2 hydrogenation with metal carbides are interesting because, depending on their carbon/metal ratio, some of them are able to adsorb CO_2 strongly and can cleave the C-O bonds in the molecule.[41,63,64,65] For example, the exposed Mo atoms in a β-Mo_2C(001)-Mo surface partially dissociate CO_2 at low temperature and the CO produced also can decompose if it overcomes a medium size energy barrier.[62,66] Thus, the hydrogenation of CO_2 on a Mo-terminated β-Mo_2C(001)-Mo can yield CO, CH_3OH and CH_4 as reaction products, see Figure 13.[65] On the other hand, a C-terminated β-Mo_2C(001)-C surface is not so aggressive for CO_2 decomposition and the ratio CO/CH_4 in the products of CO_2 hydrogenation significantly increases. On surfaces of Mo_2C, oxygen binds strongly and oxycarbides are probably the major surface species under reaction conditions.[40] Substrates such as TiC(001) and polycrystalline MoC, both with a carbon/metal ratio of one, do not dissociate CO_2 well and hydrogenation probably induces a RWGS process that eventually yields CO and methanol and no methane.[13,43] In these systems, one can alter the distribution of products by adding a metal or a metal alloy to the carbide surface.[13,40,41,43]

Strong metal-support interactions can occur after depositing metal atoms on the surface of a carbide.[37,62] Figure 14 shows electron-polarization function (ELF) plots[67] for Cu_4 and Au_4 clusters in contact with a TiC(001) substrate.[13,62] The ELF maps point to a significant relocalization of electrons in the region outside the supported Cu_4 and Au_4 clusters. This polarization of electrons is more intense in the case of Au_4. Furthermore, a Bader analysis of the charge density[68] found a net electron transfer from the TiC surface to the atoms in Cu_4 and Au_4.[13,62,69] The average charge on the metal adatoms was ~ -0.17e for Cu_4/TiC(001) and ~ -0.1e for Au_4/TiC(001).[68] The substantial electron redistribution

induced by the carbide substrate should lead to important variations with respect to the chemical properties of bulk surfaces of pure copper and gold. The phenomenon of charge polarization was only seen for single-layer metal particles where all the adatoms were directly bonded to TiC(001).[13,62,69] The redistribution of electrons was attenuated and almost disappeared once the metal particles became three dimensional.[13,62,69] Correspondingly small coverages of copper and gold on TiC(001) generated metal-carbide interfaces that were quite active for the hydrogenation of CO_2.[13]

Figure 15 displays the production of methanol on Cu(111), TiC(001), Cu/ZnO(000$\bar{1}$) and TiC(001) pre-covered with 0.1 ML of Au or Cu. Bare TiC(001) is more catalytically active than Cu(111). The Arrhenius graph gives an apparent activation energy of 20.9 kcal/mol for the production of CH_3OH on TiC(001). This apparent activation energy is smaller than the value of 25.4 kcal/mol observed for the production of CH_3OH on a Cu(111) catalyst. The calculated adsorption energy with DFT for CO_2 on the TiC(001) surface, -0.62 eV,[13] was not large but in magnitude was still bigger than binding energies found in experimental and theoretical works examining the interaction of CO_2 with copper surfaces.[4,47,49,50,51] Thus, the enhancement in catalytic activity observed in Figure 15 when going from Cu(111) to TiC(001) reflects an "upgrade" in the ability of the surface to bind CO_2. Furthermore, the complete decomposition of the adsorbate ($CO_{2,ads} \rightarrow CO_{ads} + O_a$, ΔE= -0.06 eV; $CO_{ads} + O_{ads} \rightarrow C_{ads} + 2O_{ads}$, ΔE= 1.65 eV) on titanium carbide is a highly endothermic operation. The large barrier for CO bond cleavage over TiC(001) prevents the generation of significant amounts of CH_4 as occurs during the hydrogenation of CO_2 on Mo_2C.[65]

Small coverages (< 0.15 ML) of gold and copper dispersed on TiC(001) have a catalytic activity larger than that seen for the Cu/ZnO(000$\bar{1}$) surface. As discussed below, the electronic perturbations seen for cooper and gold in contact with TiC(001) lead to a tremendous increase in the reactivity of the admetals towards CO_2. The data for Cu/TiC(001) in Figure 15 indicate that this catalyst is 5-12 times more active than Cu/ZnO(000$\bar{1}$) and 17-50 times more active than Cu(111). After normalizing the rates in Figure 15 by the total number of Cu adatoms in each sample, the TOF values on Cu/TiC(001) are 170-500 times larger than on Cu(111). A big reduction is observed for the apparent activation energy which drops from 25.4 kcal/mol on Cu(111) to 11.6 kcal/mol on Cu/TiC(001). The Au/TiC(001) system exhibits a lower catalytic activity than Cu/TiC(001) but is more active than Cu/ZnO(000$\bar{1}$), Cu(111) or TiC(001). A trend that is truly remarkable because extended surfaces of Au are not active as catalysts for the production of CH_3OH.

DFT calculations were used to investigate the adsorption of CO_2 on the Cu_4/TiC(001) and Au_4/TiC(001) model catalysts. The calculated adsorption geometries for the molecule are shown in Figure 16. CO_2 was attached to the metal adatoms in Cu_4/TiC(001) in a η^3-C,O,O configuration with a binding energy of -1.12 eV. As mentioned above, the bonding interactions of CO_2 with extended surfaces of Cu or Cu nanoparticles are very weak [4,47,51] and binding to these systems involves reaction with H adatoms during the production of CH_3OH (Figure 2).[4,47] The reduction in the strength of the C-O bonds after adsorption on Cu_4/TiC(001) is significant and dissociation of the adsorbate ($CO_{2,ads} \rightarrow CO_{ads} + O_a$) is slightly endothermic (ΔE= 0.12 eV) and more favorable than on a plain TiC(001) substrate(ΔE= 0.96 eV).[13] Thus, it appears that the

Cu_4/TiC(001) system is very efficient for activating the CO_2 molecule. On Au_4/TiC(001), the binding energy of CO_2 (-0.68 eV) was not as large as on Cu_4/TiC(001), but the binding of the molecule was still stronger than on extended surfaces of gold, copper or copper nanoparticles. This trend captures the trend experimentally observed in the activities towards CH_3OH production. Indeed, the best catalysts in Figure 15 are Cu/TiC(001) and Au/TiC(001). Their high performance for the production of CH_3OH through CO_2 hydrogenation is facilitated by the fact that they are also very active for dissociating the H_2 molecule.[13,69] On Cu_4/TiC(001) and Au_4/TiC(001), the calculated barriers for the dissociation of H_2 are 0.37 and 0.08 eV, respectively.[13,69] Thus, H_2 molecules easily can adsorb and dissociate on Cu or Au adatoms with the dissociated H migrating to the TiC surface to fill a reservoir of H atoms which are ready for the sequential hydrogenation of CO_2 at the metal-carbide interface.

V. Summary and future challenges

The hydrogenation of CO_2 to methanol is a challenging process due to the difficulties associated with the activation of CO_2[4,5,70] and possible side reactions which can produce methane and other hydrocarbons.[5,9,10] Efficient catalyst are necessary to improve the cost/benefit balance linked to the industrial use of CO_2.[5,70] The examples described above illustrate how metal-oxide (Cu-ZnO,[12,54,71] Cu-CeO_x,[11] Au-CeO_x,[57] MnO_x-CoO[14]) and metal-carbide (Cu-TiC,[13] Au-TiC[13]) interfaces can be quite useful to bind and convert CO_2 into methanol. In principle, the performance of an interface can be tuned by selecting the proper combination of metal and oxide or metal and carbide components. In these

interfaces, one can have adsorption/reaction sites of different nature with complementary chemical properties,[72,73] truly multifunctional sites which are very difficult to obtain on the surface of a pure metal or alloy systems.[4,18,19]

Although there has been significant progress in the development of catalysts for the conversion of CO_2 to methanol, there are two practical issues that must be addressed. The first one is to improve the selectivity towards methanol synthesis by reducing the amount of CO or CH_4 formed. The second one involves the desired conversion of CO_2 into higher alcohols (C2-C4). Clearly new types of metal-oxide and metal-carbide interfaces must be examined. One must optimize the properties of the metal phase and the oxide or carbide phase.

The optimization of the metal phase could involve the control of metal particle size[74] or the use of alloy systems[4,18,19,40,75] and couple them to an oxide or carbide in an attempt to obtain multifunctional catalysts. A recent theoretical study has examined the difficulties associated with the conversion of synthesis gas to methanol and ethanol on monometallic and bimetallic systems.[75] The authors highlight the fact that most higher alcohol catalysts are based on Cu or Rh, and that these metals require significant modification (via promotion with alkali, oxides, or other metals).[75] Copper is the best monometallic catalysts for the synthesis of methanol[18,75] and its performance can be improved upon forming a Cu-Zn alloy.[4,12,54] After examining the performance of several bimetallic systems for the $CO_2 \rightarrow CH_3OH$ conversion, it was found that a Ni_5Ga_5 intermetallic is particularly active and selective.[18] Comparison with conventional $Cu/ZnO/Al_2O_3$ catalysts revealed the same or better methanol synthesis activity with a

considerably lower production of CO.[18] In addition, intermetallic compounds of Pd-Gd, such as $GaPd_2$ (see Figure 17), are highly active and selective for the synthesis of CH_3OH from CO_2[76,77,78,79] Alloying also can lead to good catalysts for the production of higher alcohols.[75,80] The formation of ethanol and other higher alcohols involves the coupling of CH_x fragments to a CO molecule. CH_x species are formed via the full dissociation of CO_2 or CO followed by hydrogenation of the resulting C.[75] Pure metals are not efficient for the production of ethanol and theoretical calculations suggest that one needs alloys of the Cu_3Co, Cu_3Fe and Cu_3Co type.[75] An interesting option is to deposit these alloys on active surfaces of carbides and oxides.

For optimizing the oxide or carbide phase in the catalyst, there are several routes that involve changes in the morphology, composition and chemical state.[71,81,82,83,84,85,86] One area of research interest will be the effect of carbide stoichiometry (M_2C vs MC) and the role of oxygen binding energy on the carbide catalytic properties.[40,83] Oxide and carbide supports that contain more than one metal are interesting because in many situations they can display a catalytic performance better than that of single metal compounds.[82,84,86] Above we described the good results obtained for the CeO_x/TiO_2 system and a high performance has also been found for a hybrid oxide catalyst of manganese and cobalt.[14] Substrates such as MO_x/TiO_2 {M= V, Ru, Ce or W) display special chemical properties[84] and, thus, could be a good starting point for future studies dealing with the activation and hydrogenation of CO_2. In a recent study, the performance and metal-oxide interactions in a Cu/ZnO catalyst have been improved by doping the ZnO with Al^{3+} and Ga^{3+}, Figure 17.[71] The activity of the catalyst depends on the reducibility of ZnO and this can be affected in different ways by changing the intrinsic nature of a promoter.[71]

The approach of combining metal and oxide or carbide phases with complementary chemical properties opens up exciting routes for the generation of novel catalysts highly efficient for the hydrogenation of CO_2 to methanol or higher alcohols. The properties of a metal-oxide and metal-carbide interphases can be tuned by the use of suitable components which structurally or electronically generate the active sites necessary for the binding, activation and conversion of CO_2.

ACKNOWLEDGMENT

Many of the experiments described in the text of this article were done in collaboration with scientists at Brookhaven National Laboratory (A. Baber, J.A. Boscoboinik, J. Hrbek, S. Kattel, K. Mudiyanselage, A. Vidal, F. Xu, X. Yang, Y. Yang), the University of Seville (J. Graciani, J.F. Sanz), the University of Barcelona (L. Feria, S. Posada-Perez, F. Viñes, F. Illas), the Universidad Central de Venezuela (P. Ramirez, J. Evans) and Columbia University (M.D. Porosoff). We are grateful to all of them. This manuscript has been authored by employees of Brookhaven Science Associates, LLC under Contract No. **DE-SC0012704** with the U.S. Department of Energy.

REFERENCES

(1) Karl, T.R.; Trenberth, K.E. *Science*, **2003**, *302*, 1719-1723.

(2) Olah, G.A.; Prakash, G.K.S. ; Goeppert, A. *J. Am. Chem. Soc.* **2011**, *133*, 12881-12898.

(3) Ansari, M.B.; Min, B.-H.; Mo, Y.-H.; Park, S.-E. *Green Chem.* **2011**, *13*, 1416-1421.

(4) Behrens, M.; Studt, F.; Kasatkin, I.; Kühl, S.; Hävecker, M.; Abild-Pedersen, F.; Zander, S.; Girgsdies, F.; Kurr, P.; Kniep, B.-L.; Tovar, M.; Fischer, R. W.; Nørskov, J. K.; Schlögl, R. *Science* **2012,** *336*, 893-897.

(5) Kondratenko, E. V.; Mul, G.; Baltrusaitis, J.; Larrazabal, G. O.; Perez-Ramirez, J. *Energy Environ. Sci.* **2013**, *6*, 3112-3115.

(6) *Carbon Dioxide as Chemical Feedstock*, Aresta, M. (editor), Wiley-VCH, New York, 2010.

(7) Jadhav, S.G.; Vaidya, P.D.; Bhanage, B.M.; Joshi, J.B. *Chem. Eng. Research and Design*, **2014**, *92*, 2557-2567.

(8) Olah, G.A.; Goeppert, A.; Surya Prakash, G.K. *J. Org. Chem.* **2009**, *74*, 487-498.

(9) Miguel, C.V.; Soria, M.A.; Mendes, A.; Madeira, L.M. *J. Natural Gas Science and Eng.* **2015**, *22*, 1-8.

(10) Torrente-Murciano, L.; Mattia, D.; Jones, M.D.; Plucinski, P.K. *J. CO_2 Utilization*, 2014, 6, 34-39.

(11) Graciani, J.; Mudiyanselage, K.; Xu, F.; Baber, A. E.; Evans, J.; Senanayake, S. D.; Stacchiola, D. J.; Liu, P.; Hrbek, J.; Sanz, J. F.; Rodriguez, J. A. *Science* **2014**, *345*, 546-551.

(12) Lunkenbein, T.; Schumann, J.; Behrens, M.; Schlögl, R.; Willinger, M.G. *Angew. Chem. Int. Ed.* **2015**, *54*, 4544-4548.

(13) Vidal, A.B.; Feria, L.; Evans, J.; Takahashi, Y.; Liu, P.; Nakamura, K.; Illas, F.; Rodriguez, J.A. *J. Phys. Chem. Lett.*, **2012**, *3*, 2275.

(14) Li, C.-S.; Melaet, G.; Ralston, W.T.; An, K.; Brooks, C.; Ye, Y.; Liu, Y.-S.; Zhu, J.; Guo, J.; Alayoglu, S.; Somorjai, G.A. *Nature Communications*, **2015**, *6*, doi:10.1038/ncomms7538.

(15) Inui, T.; Hara, H.; Takeguchi, T.; Kim, J.B. *Catal. Today* **1997**, *36*, 25-32.

(16) Skrzypek, J.; Lachowska, M.; Serafin, D. *Chem. Eng. Sci.* **1990**, *45*, 89-96.

(17) Wu, J.G.; Saito, M.; Takeuchi, M.; Watanabe, T. *Appl. Catal. A : Gen.* **2001**, *218*, 235-240.

(18) Studt, F.; Sharafutdinov, I.; Abild-Pedersen, F.; Elkjær, C.; Hummelshøj, Dahl, S.; Chorkendorff, I.; Nørskov, J.K. *Nature Chemistry*, **2014**, *6*, 320-324.

(19) Yang, Y.; White, M.G.; Liu, P. *J. Phys. Chem. C*, **2012**, *116*, 248-256

(20) Kung, H.H. *Transition Metal Oxides: Surface Chemistry and Catalysis*, Elsevier: New York, 1989.

(21) Staudt, T.; Lykhach, Y.; Tsud, N.; Skála, T. S.; Prince, K. C.; Matolín, V. R.; Libuda, J. R. *J. Phys. Chem. C* **2011**, *115*, 8716-8721.

(22) Zhang, Z.; Verykios, X. *Catal. Lett.* **1996**, *38*, 175-183.

(23) Park, J. B.; Graciani, J.; Evans, J.; Stacchiola, D.; Ma, S.; Liu, P.; Nambu, A.; Sanz, J. F.; Hrbek, J.; Rodriguez, J. A. *Proc. Natl. Acad. Sci* **2009**, *106*, 4975-4981.

(24) Pacchioni, G.; Freund, H.-J. *Chem. Rev*. **2013**, *113*, 4035-4075.

(25) Stacchiola, D.; Senanayake, S.; Liu, P.; Rodriguez, J.A. *Chem. Rev.* **2013**, *113*, 4373-4390.

(26) Surnev, S.; Fortunelli, A; Netzer, F.P. *Chem. Rev.* **2013**, *113*, 4314-4372.

(27) Martynova, Y.; Liu, B.-H.; McBriarty, M.E.; Groot, I.M.N.; Bedzyk, M.J.; Shaikhutdinov, S.; Freund, H.-J. *J. Catal.* **2013**, *301*, 227-232.

(28) Park, J. B.; Graciani, J.; Evans, J.; Stacchiola, D.; Senanayake, S. D.; Barrio, L.; Liu, P.; Sanz, J. F.; Hrbek, J.; Rodriguez, J. A. *J. Am. Chem. Soc.* **2009**, *132*, 356-361.

(29) Graciani, J.; Plata, J. J.; Sanz, J. F.; Liu, P.; Rodriguez, J. A. *J. Chem. Phys.* **2010**, *131*, 104703.

(30) Mudiyanselage, K.; Senanayake, S.D.; Feria, L.; Kundu, S.; Baber, A.; Graciani, J.; Vidal, A.B.; Agnoli, S.; Evans, J.E.; Chang, R.; Axnada, S.; Liu, Z.; Sanz, J.F.; Liu, P.; Rodriguez, J.A.; Stacchiola, D. *Angew. Chem Int. ed.* **2013**, 52, 5101-5105.

(31) Wrobel, R.; Suchorski, Y.; Becker, S.; Weiss, H. *Surf. Sci.* **2008**, *602*, 436-442.

(32) Campbell, C.T. *Surf. Sci. Reports* **1997**, *27*, 1-111.

(33) Campbell, C.T. *Nature Chemistry*, **2012**, *4*, 597-598.

(34) Solymosi, F. *Journal of Catalysis* **1985,** *94*, 581-585.

(35) Bruix, A.; Rodriguez, J. A.; Ramírez, P. J.; Senanayake, S. D.; Evans, J.; Park, J. B.; Stacchiola, D.; Liu, P.; Hrbek, J.; Illas, F. *J. Ame. Chem. Soc.* **2012,** *134*, 8968-8974.

(36) Acerbi, N.; Tsang, S. C. E.; Jones, G.; Golunski, S.; Collier, P. *Angew. Chem. Int. Ed.* **2013,** *52*, 7737-7741.

(37) Rodriguez, J.A.; Illas, F. *Phys. Chem. Chem. Phys.* **2012**, *14*, 427-438.

(38) Schweizer, N.M.; Schaidle, J.A.; Ezekoye, O.K.; Pan, X.; Linic, S.; Thompson, L.T. *J. Am. Chem. Soc.* **2011**, *133*, 2378-2381.

(39) Hwu, H.; Chen, J.G. *Chem. Rev.* **2005**, *105*, 185-202.

(40) Porosoff, M.D.; Yang, X.; Boscoboinik, J.A.; Chen, J.G. *Angew. Chem. Int. Ed*. **2014**, *53*, 6705-6709.

(41) Dubois, J.-L.; Sayama, K.; Arakawa, H. *Chem. Letters*, **1992**, 5-8.

(42) Wu, S.-Y.; Ho, J.-J. *J. Phys. Chem. C*, **2012**, *116*, 13202-13209.

(43) Rodriguez, J.A.; Evans, J.; Feria, L.; Vidal, A.B.; Liu, P.; Nakamura, K.; Illas, F. *J. Catal.* **2013**, *307*, 162-163.

(44) Rasmussen, P.B.; Holmblad, P.M.; Askgaard, T.; Ovesen, C.V.; Stoltze, P.; Nørskov, J.K.; Chorkendorff, I. *Catal. Lett*. **1994**, *26*, 373-379.

(45) Rasmussen, P.B.; Kazuta, M.; Chorkendorff, I. *Surf. Sci*. **1994**, *318*, 267.

(46) Yoshihara, J.; Campbell, C.T. *J. Catal*. **1996**, *161*, 776.

(47) Yang, Y.; Evans, J.; Rodriguez, J.A.; White, M.G.; Liu, P. *Phys. Chem. Chem. Phys*. **2010**, *12*, 9909-9917.

(48) Szanyi, J.; Goodman, D.W. *Catal. Lett.* **1991**, *10*, 383-390.

(49) Nakamura, J.; Rodriguez, J.A.; Campbell, C.T. *J. Phys.: Condens. Matter* **1989**, *1*, SB 149.

(50) Schneider, T.; Hirschwald, W. *Catal. Lett.* **1992**, *14*, 197-204.

(51) Grabow, L.C.; Mavrikakis, M *ACS Catal*. **2011**, *1*, 365-384.

(52) Rodriguez, J.A.; Clendening , W.D.; Campbell, C.T. *J. Phys. Chem.* **1989**, *93*, 5238.

(53) Koplitz, L.V.; Dulub, O.; Diebold, U. *J. Phys. Chem. B*, **2003**, *107*, 10583-10590.

(54) Nakamura, J.; Nakamura, I.; Uchijima, T.; Kanai, Y.; Watanabe, T.; Saito, M.; Fujitani, T. *J. Catal.* **1996**, *160*, 65-75.

(55) Yang, F.; Choi, Y.M.; Agnoli, S,; Liu, P.; Stacchiola, D.; Hrbek, J.; Rodriguez, J.A. *J. Phys. Chem. C*, **2011**, *115*, 23062-23066.

(56) Yang, Y.; Mims, C.A.; Mei, D.H.; Peden, C.H.F.; Campbell, C.T. *J. Catal.* **2013,** *298*, 10-19.

(57) Yang, X.; Kattel, S.; Senanayake, S.D.; Boscoboinik, J.A.; Nie, X.; Graciani, J.; Rodriguez, J.A.; Liu, P.; Stacchiola, D.J.; Chen, J.G. *J. Am. Chem. Soc.* **2015**, *137*, 10104-10107.

(58) Ono, L.K.; Sudfeld, D.; Roldan Cuenya, *Surf. Sci.* **2006**, *600*, 5041.

(59) *Chemistry of Transition Metal Carbides and Nitrides,* Oyama, S.T. (editor), Springer, Berlin, 1996.

(60) Levy, R.B. ; Boudart, M. *Science,* **1973**, *181*, 547-551.

(61) Furimsky, E. *Applied Catal. A: General*, **2003** , *240*, 1-28.

(62) Rodriguez, J.A.; Viñes, F.; Illas, F.; Liu, P.; Takahashi, Y.; Nakamura, K. *J. Chem. Ph ys.* **2007**, *127*, 211102-211105.

(63) Stottlemyer, A.L.; Kelly, T.G.; Meng, Q.; Chen, J.G. *Surf. Sci. Reports*, **2012**, *67*, 201-232.

(64) Solymosi, F.; Oszkó, A.; Bánsági, T.; Tolmacsov, P. *J. Phys. Chem. B*, **2002**, *106*, 9613-9618.

(65) Posada-Pérez, S.; Viñes, F.; Ramirez, P.J.; Vidal, A.B.; Rodriguez, J.A.; Illas, F. *Phys. Chem. Chem. Phys.* **2014**, *16*, 14912-14921.

(66) Wang, T.; Li, Y.W.; Wang, J.; Beller, M.; Jiao, H. *J. Phys. Chem. C*, **2014**, *118*, 3162.

(67) Silvi, B.; Savin, A. *Nature*, **1994**, *371*, 683-686.

(68) Bader, R. *Chem. Rev.* **1991**, *91*, 893-928.

(69) Gomez, T.; Florez, E.; Rodriguez, J.A.; Illas, F. *J. Phys. Chem. C*, **2011**, *115*, 11666-11672.

(70) Quadrelli, A.; Centi, G.; Duplan, J.-L.; Perathoner, S. *Chem. Sus. Chem.* **2011**, *4*, 1194-1215.

(71) Schumann, J.; Eichelbaum, M.; Lunkenbein, T.; Thomas, N.; Álvárez-Galvan, M.C.; Schlögl, R.; Behrens, M. *ACS Catal.* **2015**, *5*, 3260-3270.

(72) Green, I.X.; Tang, W.; Neurock, M.; Yates, J.T. *Science*, **2011**, 333, 736-739.

(73) Behrens, M. *Angew. Chem. Int. Ed.* **2014**, *53*, 12022-12024.

(74) James, T.E.; Hemmingson, S.L.; Campbell, C.T. *ACS Catal.* **2015**, *5*, 5673-5678.

(75) Medford, A.J.; Lausche, A.C.; Abild-Pedersen, F.; Temel, B.; Schjødt, N.C.; Nørskov, J.K.; Studt, F. *Top. Catal*. **2014**, *57*, 135-142.

(76) Fujitani, T.; Saito, M.; Kanai, Y.; Watanabe, T.; Nakamura, J.; Uchijima, T. *Appl. Catal. A*, **1995**, *125*, L199-202.

(77) Ota, A.; Kunkes, E.L.; Kasatkin, I.; Groppo, E.; Ferri, D,; Poceiro, B.; Navarro, R,M.; Yerga, S.; Behrens, M. *J. Catal.* **2012**, *293*, 27-38.

(78) Chiavassa, D.L.; Collins, S.E.; Bonivardi, A,L.; Baltanas, M.A. *Chem. Eng. J.* **2009**, *150*, 204-212.

(79) Fiordaliso, E.M.; Sharafutdinov, I.; Carvalho, H.W.P.; Grunwaldt, J.-D.; Hansen, T.W.; Chorkendorff, I.; Wagner, J.B.; Damsgaard, C.D. *ACS Catal.* **2015**, *5*, 5827-5836.

(80) Xiang, Y.; Barbosa, R.; Kruse, N. *ACS Catalysis*, **2014**, *4*, 2792-2800.

(81) Xu, W.; Ramirez, P.J.; Stacchiola, D.; Rodriguez, J.A. *Catal. Lett.* **2014**, *144*, 1418-1424.

(82) He, G.; Yan, Z.; Ma, X.; Meng, H.; Shen, P.K.; Wang, C. *Nanoscale*, **2011**, *3*, 3578-3582.

(83) Porosoff, M.D.; Kattel, S.; Li, W.; Liu, P.; Chen, J.G. *Chem. Comm.* **2015**, *51*, 6988-6991.

(84) Stacchiola, D.J.: Senanayake, S.D.: Liu, P.; Rodriguez, J.A. *Chemical Reviews*, **2013**, *113*, 4373-4390.

(85) Reddy, B.J.; Khan, A. *Catalysis Reviews: Science & Engineering*, **2005**, *47*, 257-296.

(86) Misono, M. *Heterogeneous Catalysis of Mixed Oxides*, Elsevier: New York, 2013.

Figure captions

Figure 1 Arrhenius plot for methanol synthesis (dark filled symbols) and the reverse water-gas shift reaction (empty symbols) over Cu(111) and a ZnO(000$\bar{1}$) surface pre-covered with 0.2 ML of copper. In a batch reactor, the catalysts were exposed to 0.049 MPa (0.5 atm) of CO_2 and 0.441 MPa (4.5 atm) of H_2. The reported values are steady-state rates measured at temperatures of 600, 575, 550, 525 and 500 K, with a total conversion below 10 % (reproduced from ref. 47, Copyright 2010 Royal Society of Chemistry).

Figure 2 Possible reaction pathways for CO_2 hydrogenation on (reproduced from ref. 47, Copyright 2010 Royal Society of Chemistry).

Figure 3 Potential energy diagram for the methanol synthesis reaction on the Cu(111) surface and Cu_{29} nanoparticle, where the thin bar represents the intermediates and the thick bar represents the transition states. The upper diagram corresponds to Cu(111) and the lower diagram corresponds to Cu_{29} (reproduced from ref. 47, Copyright 2010 Royal Society of Chemistry).

Figure 4 Part A: Turnover frequency (TOF) for methanol formation after depositing different coverages of ZnO_x on a surface of polycrystalline copper.[54] The hydrogenation of CO_2 was carried out at 523 K and a total pressure of 18 atm (reproduced from ref. 54, Copyright 1996 Elsevier). Part B: Oxide/metal configuration for model catalysts used in the study of the synthesis of methanol through CO_2 hydrogenation.

Figure 5 Part A: Growth of ceria particles on Cu(111). Part B: In a batch reactor, Cu(111) and a surface covered 20% by ceria were exposed to 0.049 MPa (0.5 atm) of CO_2 and 0.441 MPa (4.5 atm) of H_2. The reported values are steady-state rates measured at temperatures of 600, 575, 550, 525 and 500 K with total conversion below 10%.

Figure 6 IRRA spectra at ambient pressures. The spectra were obtained following the exposure of CeO_x/Cu(111) to CO_2 and H_2 at the indicated pressures and temperatures. All the spectra except the one at the bottom were collected in the presence of CO_2 or a CO_2 + H_2 mixture at the indicated pressures (reproduced from ref. 11, Copyright 2014 AAAS).

Figure 7 Part A: Ce_6O_{13} clusterused for the modeling of a CeO_x/Cu(111) catalyst. Part B: Calculated adsorption geometry for CO_2 on CeO_x/Cu(111).

Figure 8 STM image for the type of $CeO_x/TiO_2(110)$ substrate used to generate $Cu/CeO_x/TiO_2(110)$ and $Au/CeO_x/TiO_2(110)$ catalysts (reproduced from ref. 28, Copyright 2009 American Chemical Society).

Figure 9 Arrhenius plot for methanol synthesis on Cu(111), 0.2 ML of Cu on ZnO(000$\bar{1}$), a Cu(111) surface covered 20% by ceria, and 0.1 ML of Cu on a $TiO_2(110)$ surface pre-covered 15% with ceria. In a batch reactor the catalysts were exposed to 0.5

atm of CO_2 and 4.5 atm of H_2. The reported values are steady-state rates measured at 600, 575, 550, 525 and 500 K with a total conversion below 10% (reproduced from ref. 11, Copyright 2014 AAAS).

Figure 10 Production of methanol and CO over $Cu/TiO_2(110)$, $Cu/CeO_x/TiO_2(110)$, $Au/TiO_2(110)$ and $Au/CeO_x/TiO_2(110)$ catalysts. The partial pressures of the two products are plotted. T= 573 K, 110 mTorr of CO_2 and 700 mTorr of H_2 (taken from ref. 57, Copyright 2015 American Chemical Society).

Figure 11 Reaction energetics calculated by DFT for the hydrogenation of CO_2 on $Au_3/TiO_2(110)$ and $Au_3/CeO_x/TiO_2(110)$ surfaces. "TS" denotes the transition states (reproduced from ref. 57, Copyright 2015 American Chemical Society).

Figure 12 Model used to represent a $Au/CeO_x/TiO_2(110)$ surface. A Au_3 cluster was deposited on a $CeO_x/TiO_2(110)$ surface. The numbers denote the net Bader charges. Color code: Yellow (gold), green (cerium), red (oxygen) and blue (titanium). (Reproduced from ref. 57, Copyright 2015 American Chemical Society).

Figure 13 Arrhenius plot for the production of CO, methane and methanol on β-$Mo_2C(001)$-Mo. In a batch reactor, the metal carbide catalysts was exposed to 0.049 MPa (0.5 atm) of CO_2 and 0.441 MPa (4.5 atm) of H_2 at temperatures of 600, 575, 550, 525 and 500 K with a total conversion below 10% (reproduced from ref. 65, Copyright 2014 Royal Society of Chemistry).

Figure 14 Electron-polarization plots for Cu_4 (left) and Au_4 (right) supported on TiC(001). The metal adatoms are adsorbed on C sites of TiC(001). The probability of finding electron pairs varies from 0 (blue color) to 1 (red color). Thus, the green shape above the metal particle denotes a substantial probability of electron pair localization. (Reproduced from ref. 13, Copyright 2012 American Chemical Society).

Figure 15 Arrhenius plot for methanol synthesis on Cu(111), a ZnO(000$\bar{1}$) surface pre-covered with 0.2 ML of Cu, clean TiC(001) and titanium carbide pre-covered with 0.1 ML of Au or Cu. In a batch reactor, the catalysts were exposed to 0.049 MPa (0.5 atm) of CO_2 and 0.441 MPa (4.5 atm) of H_2. The reported values are for steady state rates measured at temperatures of 600, 575, 550, 525 and 500 K with a total conversion below 10%. (Reproduced from ref. 13, Copyright 2012 American Chemical Society).

Figure 16 Calculated adsorption geometries for CO_2 on $Au_4/TiC(001)$ and $Cu_4/TiC(001)$. Color code: Oxygen (red), carbon (light grey), titanium (dark blue), gold (yellow), copper (light blue). (Reproduced from ref. 13, Copyright 2012 American Chemical Society).

Figure 17 Left side: Turnover frequency (TOF) for $GaPd_2/SiO_2$ and $CuZnO/Al_2O_3$ catalysts as a function of temperature. Right side: High resolution TEM of a $GaPd_2$

nanoparticle acquired in an environmental TEM under reducing conditions (823 K, 3 Torr of H_2). (Reproduced from ref. 79, Copyright 2015 American Chemical Society).

Figure 18 Left side: Cartoon illustrating the migration of ZnO_x agregates to the top of Cu particles in Cu/ZnO and Cu/ZnO:M catalysts (M= Al^{3+} and Ga^{3+}). Such migration is not observed for the Cu/ZnO:Mg catalyst. Right side: Activity, weight time yield, of Cu/ZnO and Cu/ZnO:M catalysts for methanol synthesis. (Reproduced from ref. 71, Copyright 2015 American Chemical Society).

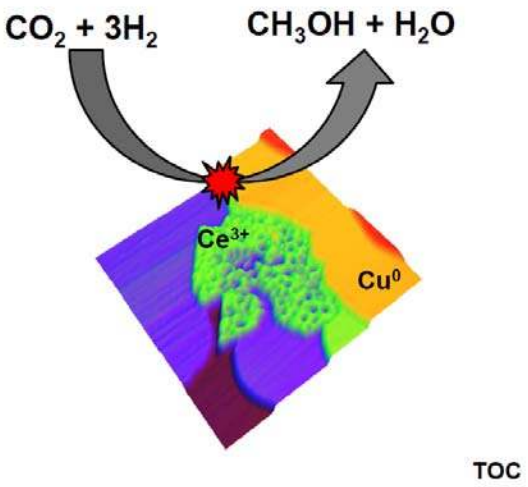

TOC

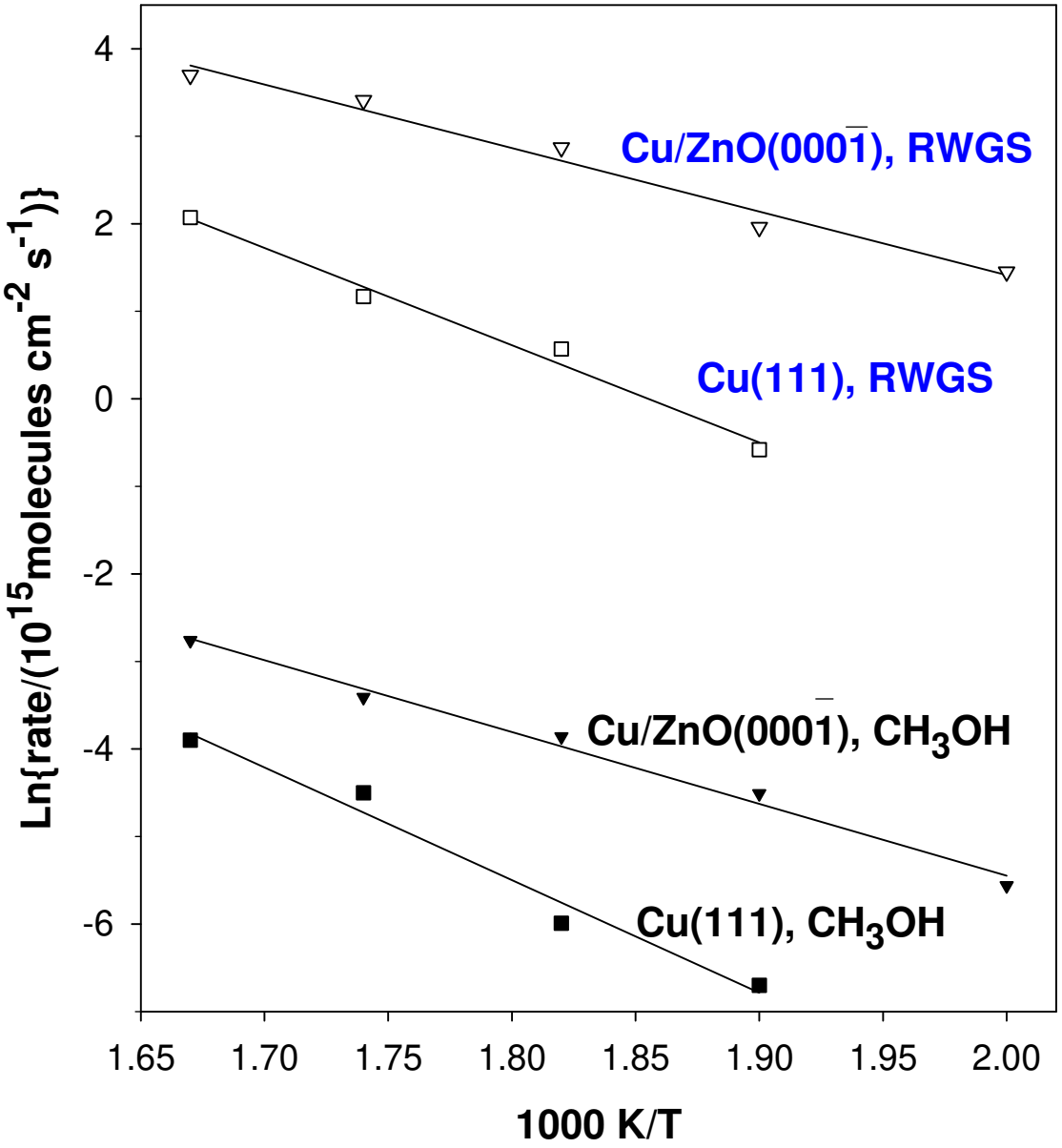
Cu/ZnO(000$\bar{1}$), RWGS
Cu(111), RWGS
Cu/ZnO(000$\bar{1}$), CH_3OH
Cu(111), CH_3OH
Ln{rate/(10^{15}molecules cm^{-2} s^{-1})}
1000 K/T
4
2
0
-2
-4
-6
1.65
1.70
1.75
1.80
1.85
1.90
1.95
2.00

Fig 1

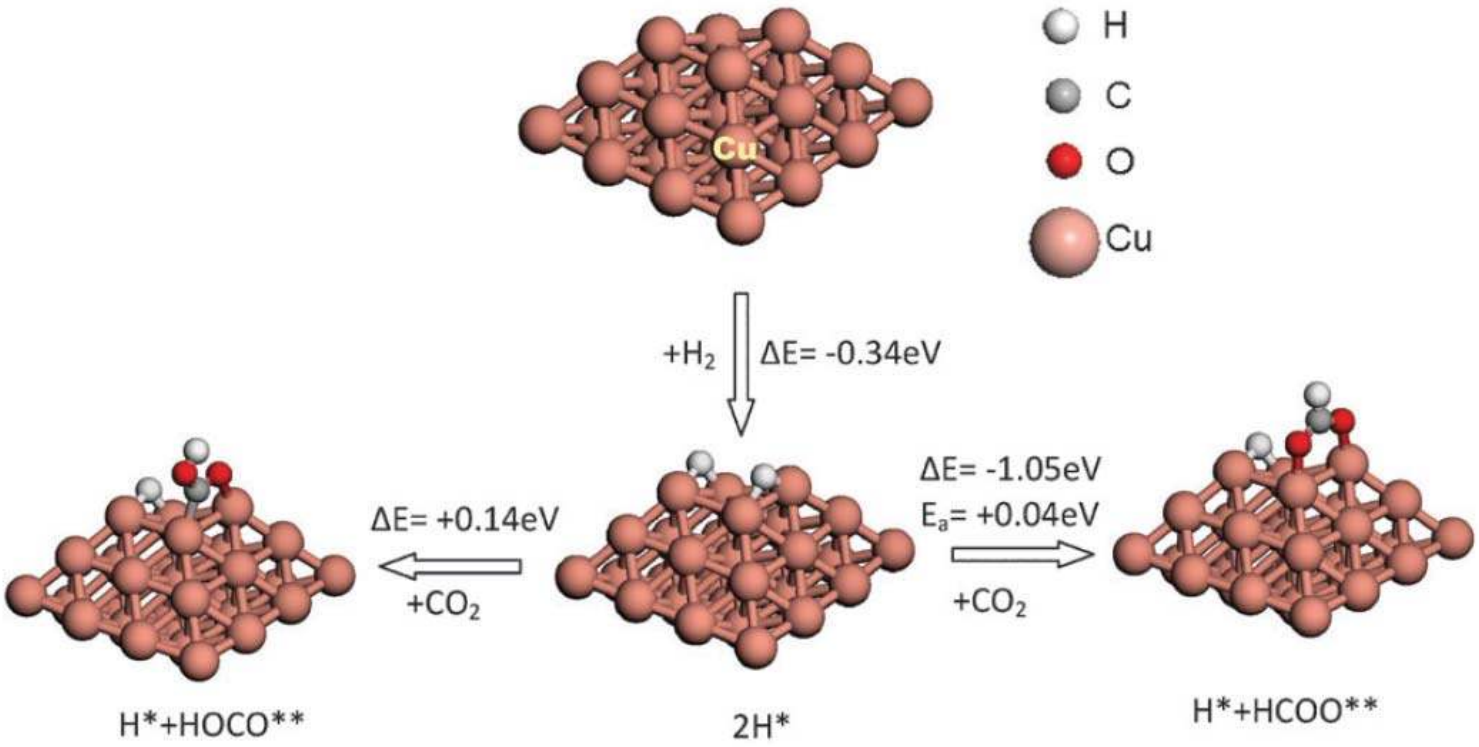
H
C
O
Cu
Cu
+H2
ΔE= -0.34eV
ΔE= +0.14eV
+CO2
ΔE= -1.05eV
Ea= +0.04eV
+CO2
H*+HOCO**
2H*
H*+HCOO**

Figure 2

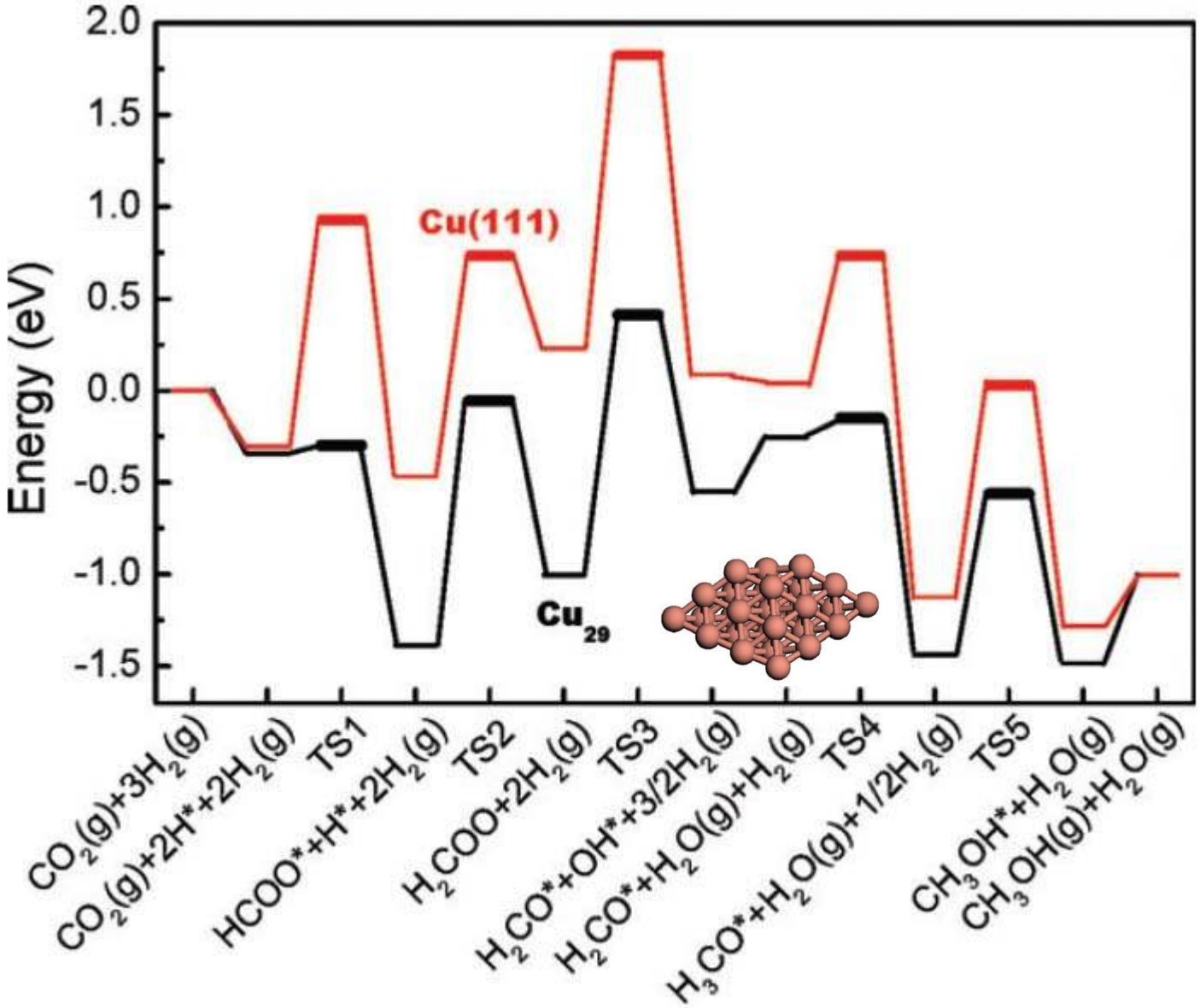
Energy (eV)
2.0
1.5
1.0
0.5
0.0
-0.5
-1.0
-1.5
Cu(111)
Cu29
CO2(g)+3H2(g)
CO2(g)+2H*+2H2(g)
TS1
HCOO*+H*+2H2(g)
TS2
H2COO+2H2(g)
TS3
H2CO*+OH*+3/2H2(g)
H2CO*+H2O(g)+H2(g)
TS4
H3CO*+H2O(g)+1/2H2(g)
TS5
CH3OH*+H2O(g)
CH3OH(g)+H2O(g)

Figure 3

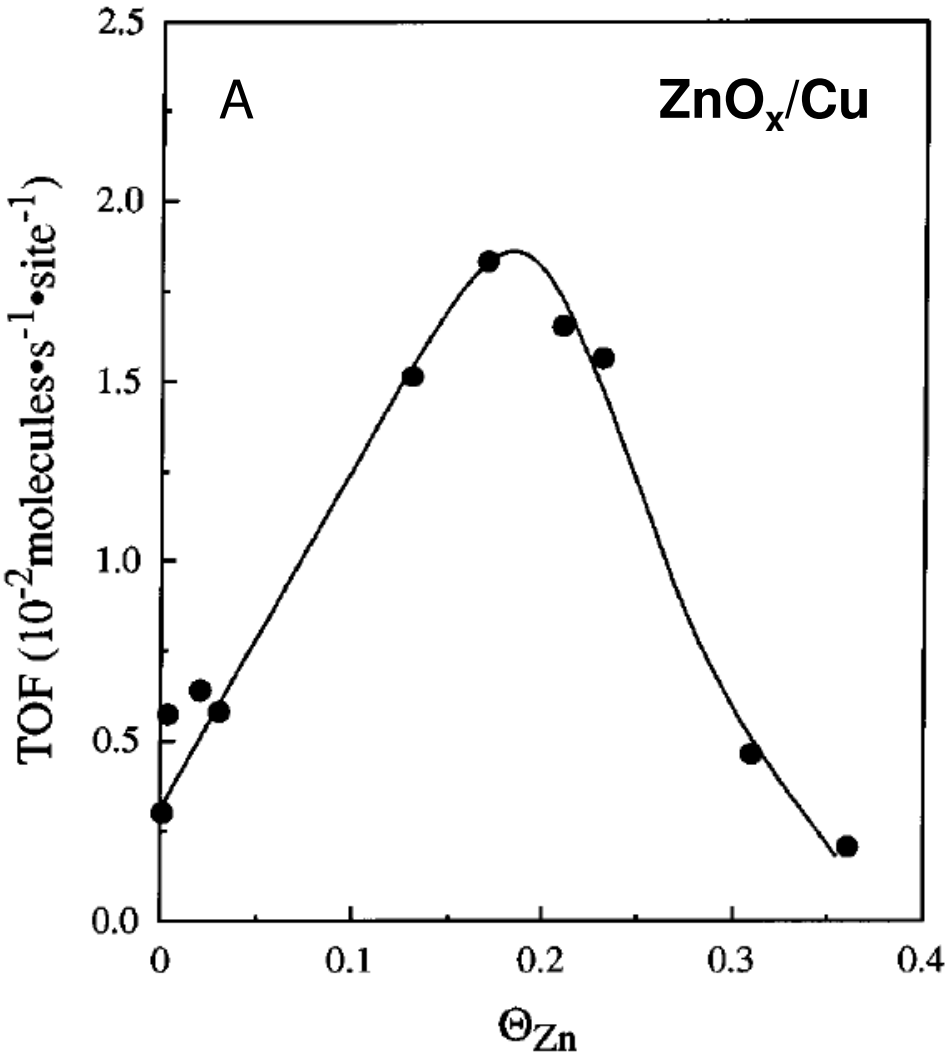
A
ZnO_x/Cu
TOF (10^{-2}molecules•s^{-1}•site^{-1})
2.5
2.0
1.5
1.0
0.5
0.0
0
0.1
0.2
0.3
0.4
Θ_{Zn}

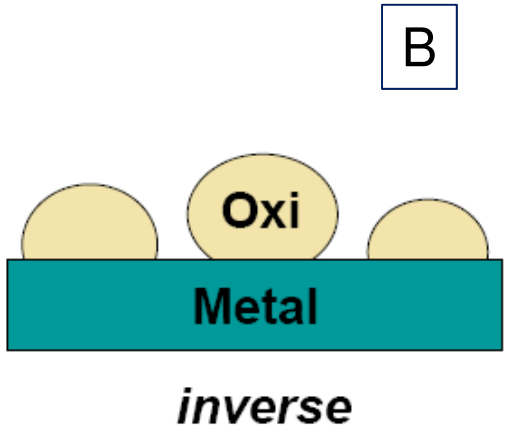
B
Oxi
Metal
inverse

Figure 4

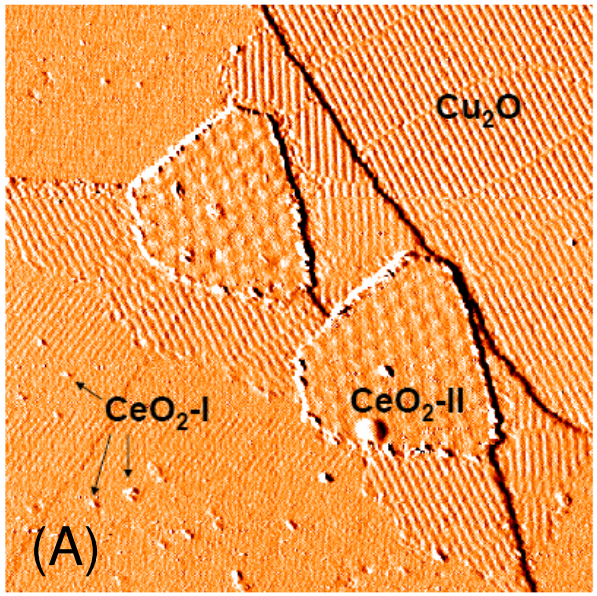

150nm x 150nm

AP-XPS under reaction

$Cu^{1+} \rightarrow Cu^0$

$Ce^{4+} \rightarrow Ce^{3+}$

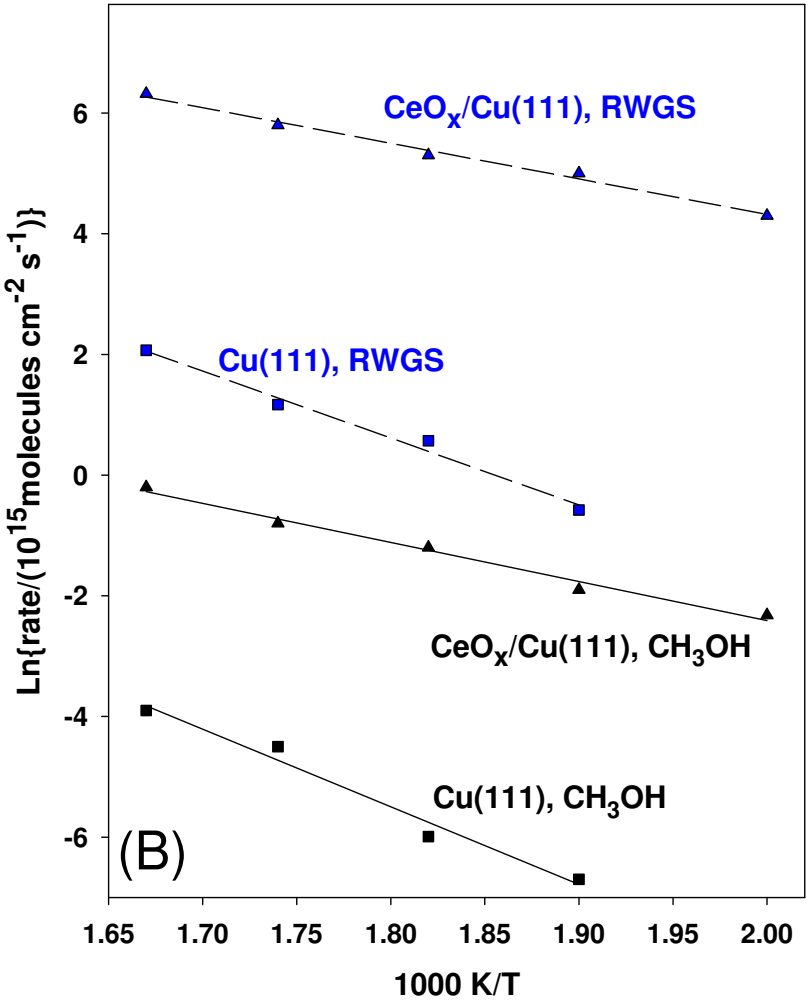

Figure 5

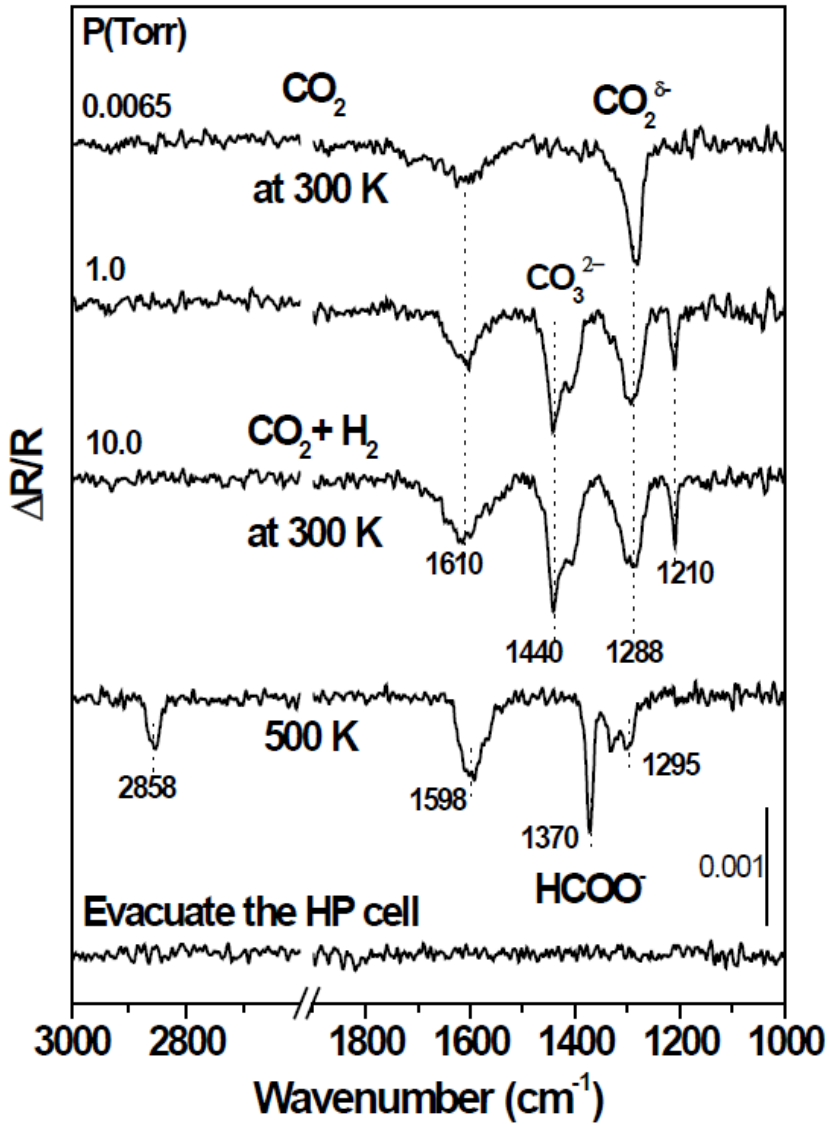
P(Torr)
0.0065
CO2
CO2 δ-
at 300 K
1.0
CO3 2−
10.0
CO2 + H2
at 300 K
1610
1440
1288
1210
500 K
2858
1598
1370
1295
HCOO-
0.001
Evacuate the HP cell
ΔR/R
3000
2800
1800
1600
1400
1200
1000
Wavenumber (cm-1)

Figure 6

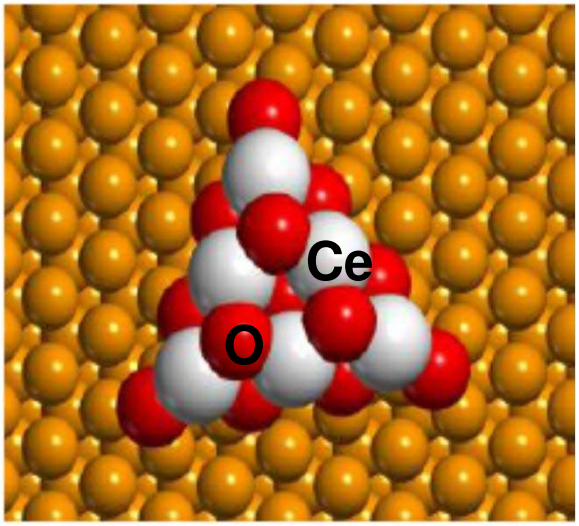

(A)

(B)

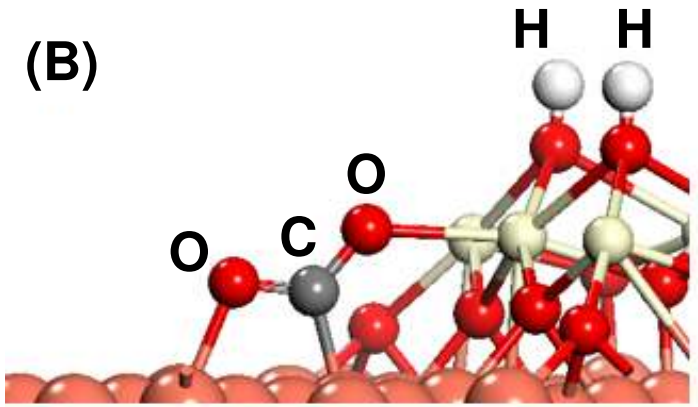

Ce_6O_{13}

Cu(111)

Figure 7

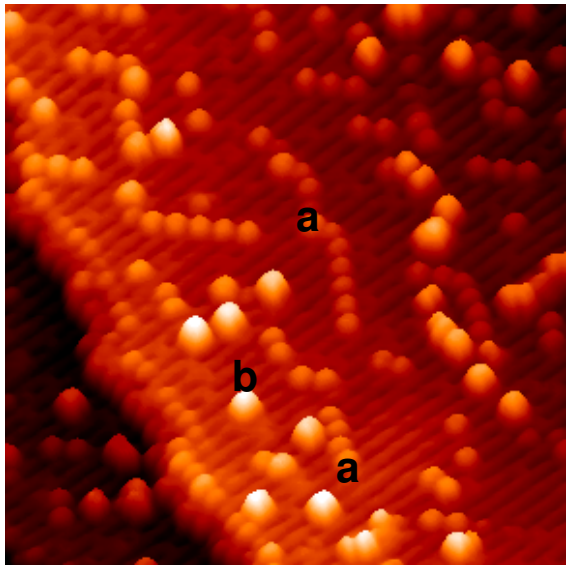

20 nm x 20 nm

a= CeO_x site ; b= TiO_x site

$CeO_x/TiO_2(110)$

Figure 8

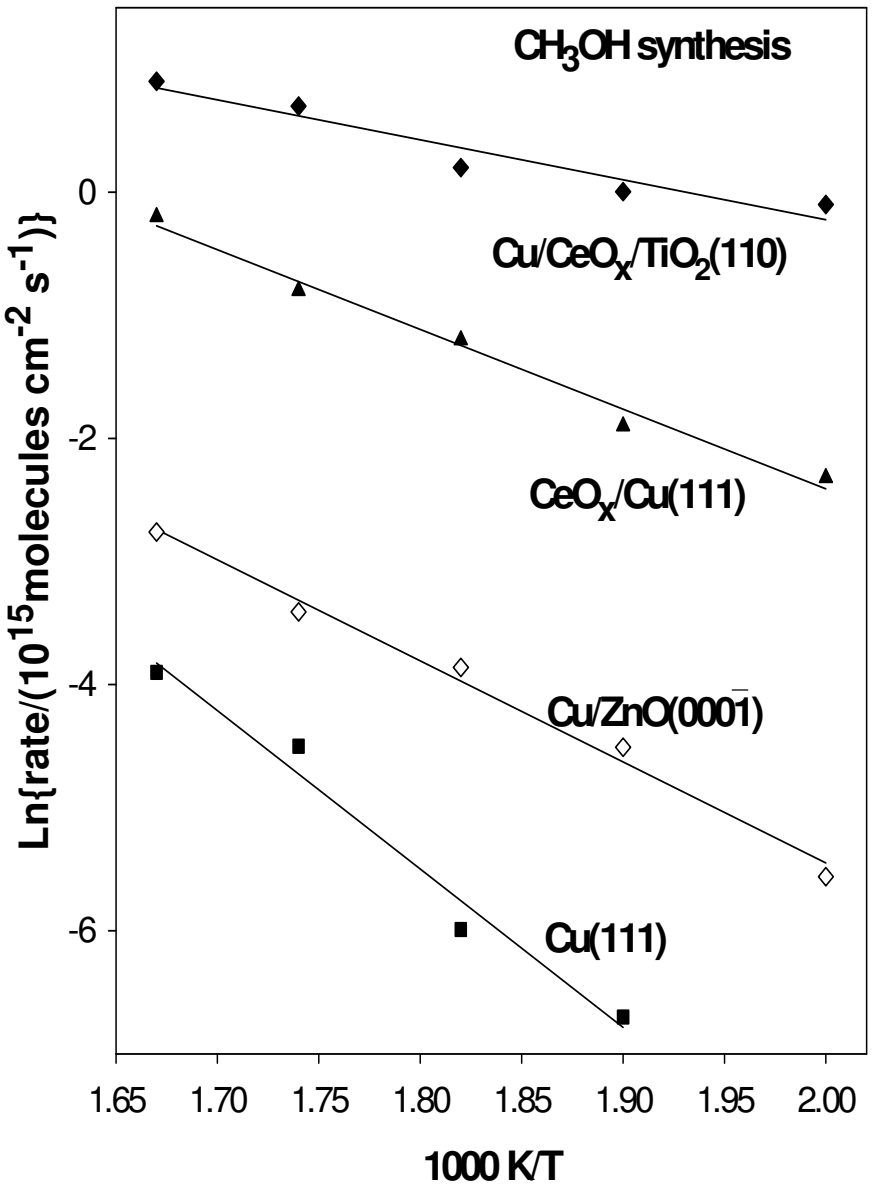
CH3OH synthesis
Cu/CeOx/TiO2(110)
CeOx/Cu(111)
Cu/ZnO(000$\bar{1}$)
Cu(111)
0
-2
-4
-6
1.65
1.70
1.75
1.80
1.85
1.90
1.95
2.00
1000 K/T
Ln{rate/(10^15 molecules cm^-2 s^-1)}

Figure 9

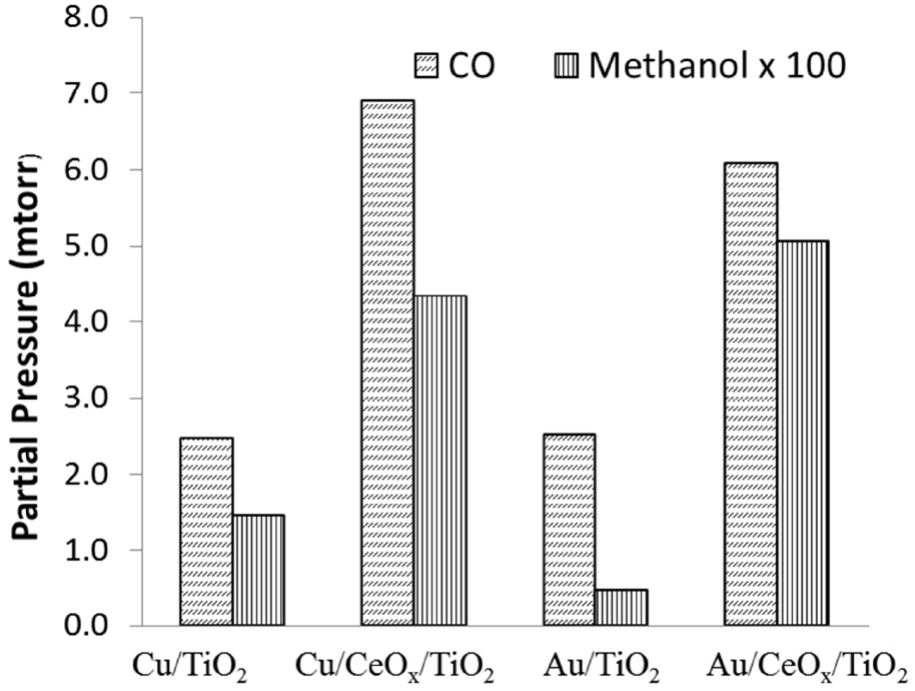
8.0
7.0
6.0
5.0
4.0
3.0
2.0
1.0
0.0
Partial Pressure (mtorr)
CO
Methanol x 100
Cu/TiO2
Cu/CeOx/TiO2
Au/TiO2
Au/CeOx/TiO2

Figure 10

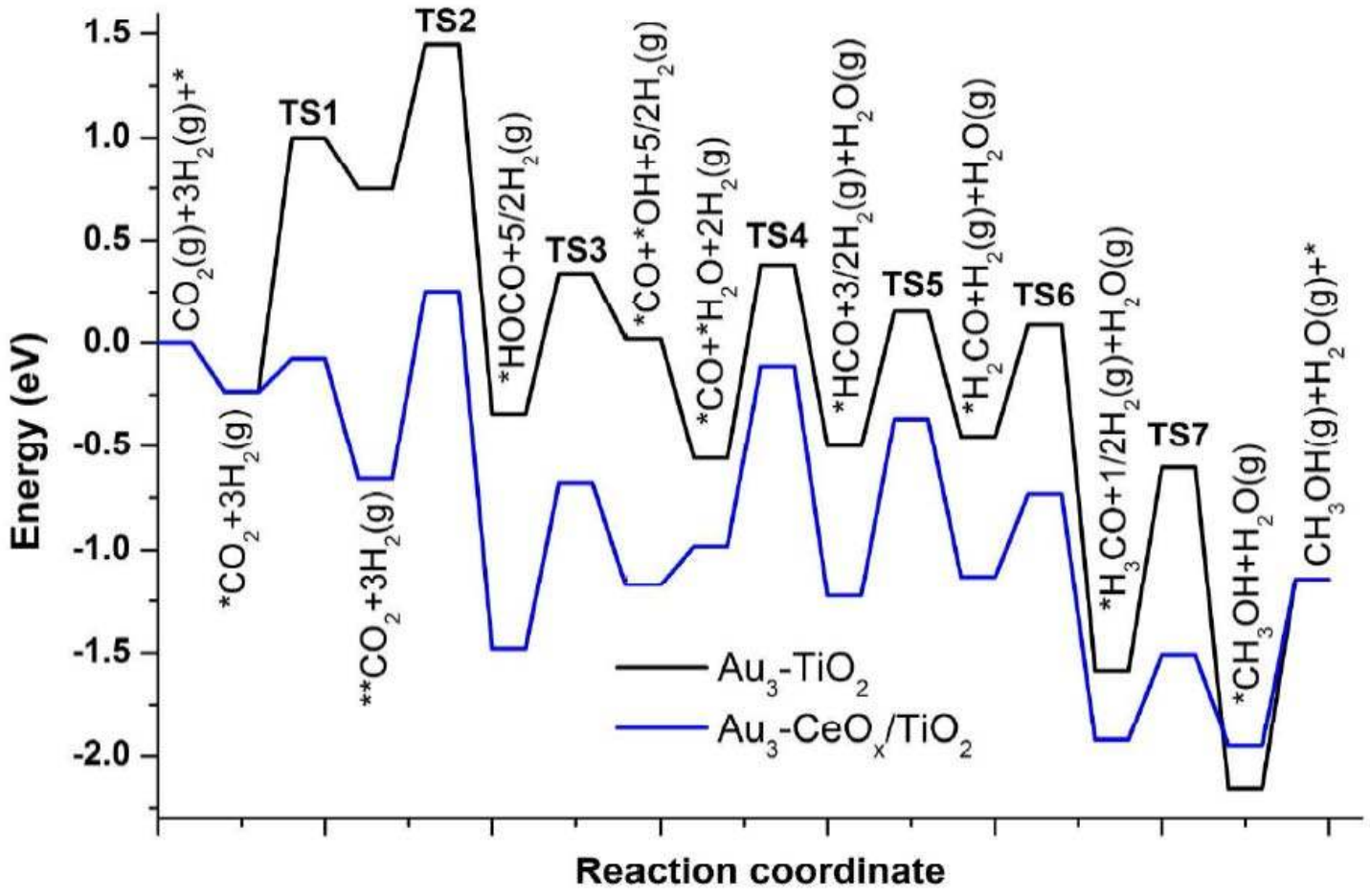
Energy (eV)
1.5
1.0
0.5
0.0
-0.5
-1.0
-1.5
-2.0
TS1
TS2
TS3
TS4
TS5
TS6
TS7
$CO_2(g)+3H_2(g)+*$
$*CO_2+3H_2(g)$
$**CO_2+3H_2(g)$
$*HOCO+5/2H_2(g)$
$*CO+*OH+5/2H_2(g)$
$*CO+*H_2O+2H_2(g)$
$*HCO+3/2H_2(g)+H_2O(g)$
$*H_2CO+H_2(g)+H_2O(g)$
$*H_3CO+1/2H_2(g)+H_2O(g)$
$*CH_3OH+H_2O(g)$
$CH_3OH(g)+H_2O(g)+*$
Au_3-TiO_2
Au_3-CeO_x/TiO_2
Reaction coordinate

Figure 11

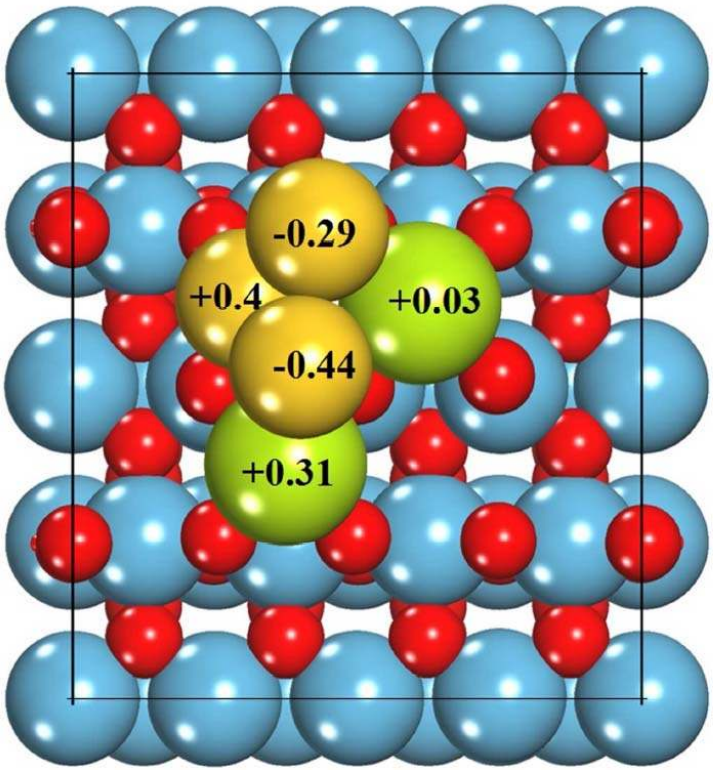

Figure 12

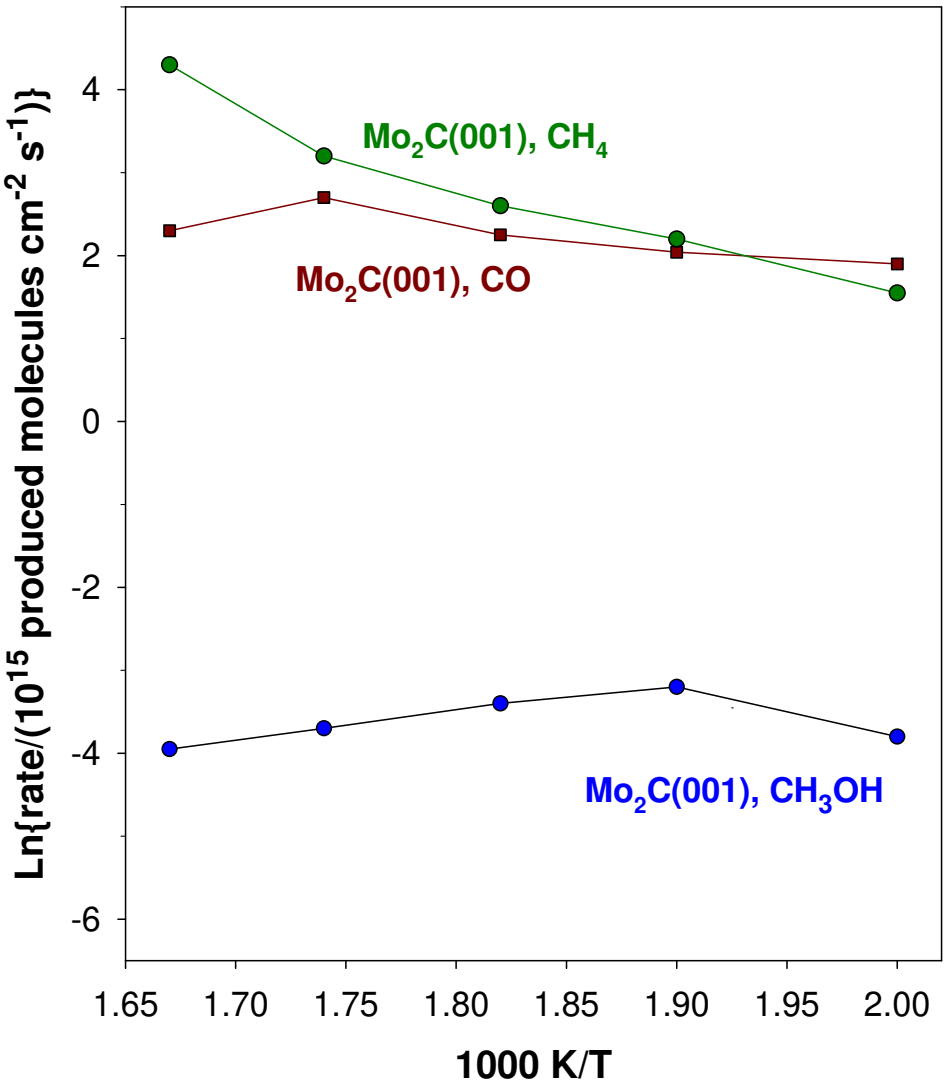
Ln{rate/(10^15 produced molecules cm^-2 s^-1)}
4
2
0
-2
-4
-6
Mo2C(001), CH4
Mo2C(001), CO
Mo2C(001), CH3OH
1.65
1.70
1.75
1.80
1.85
1.90
1.95
2.00
1000 K/T

Figure 13

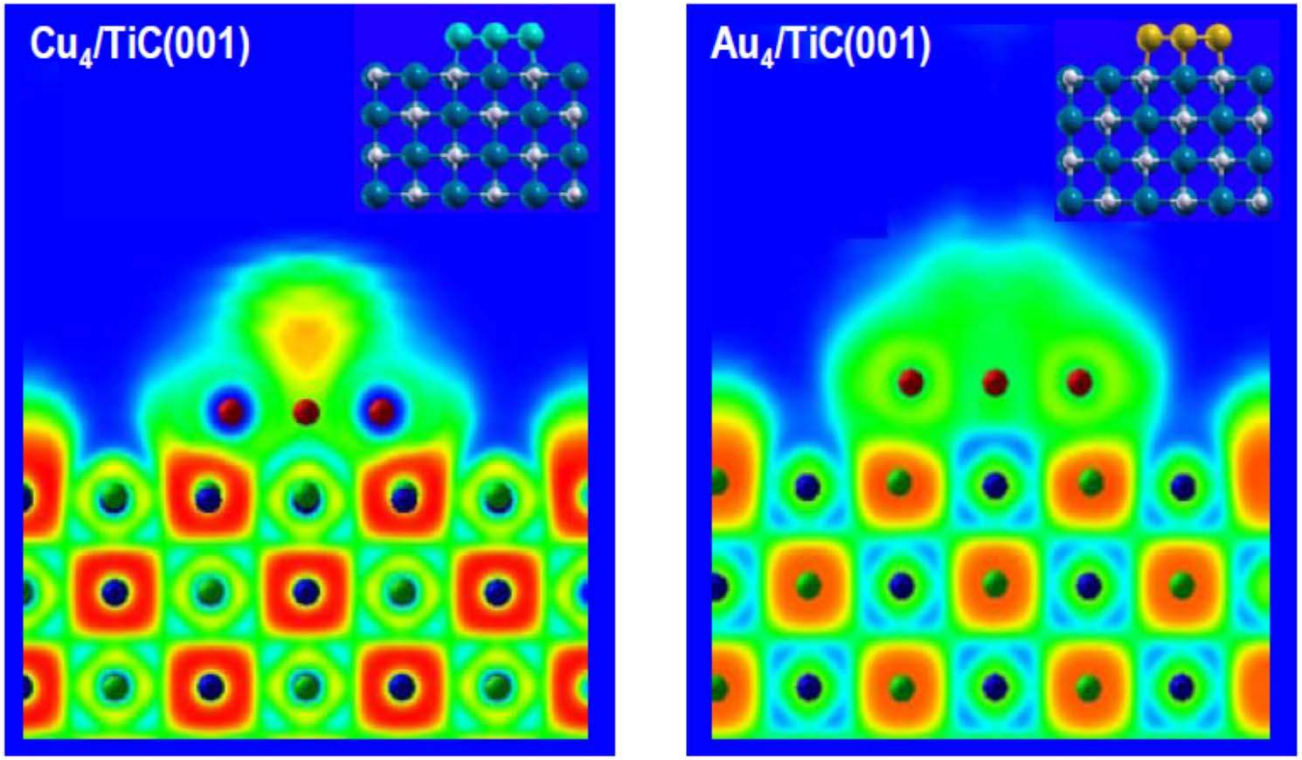

Figure 14

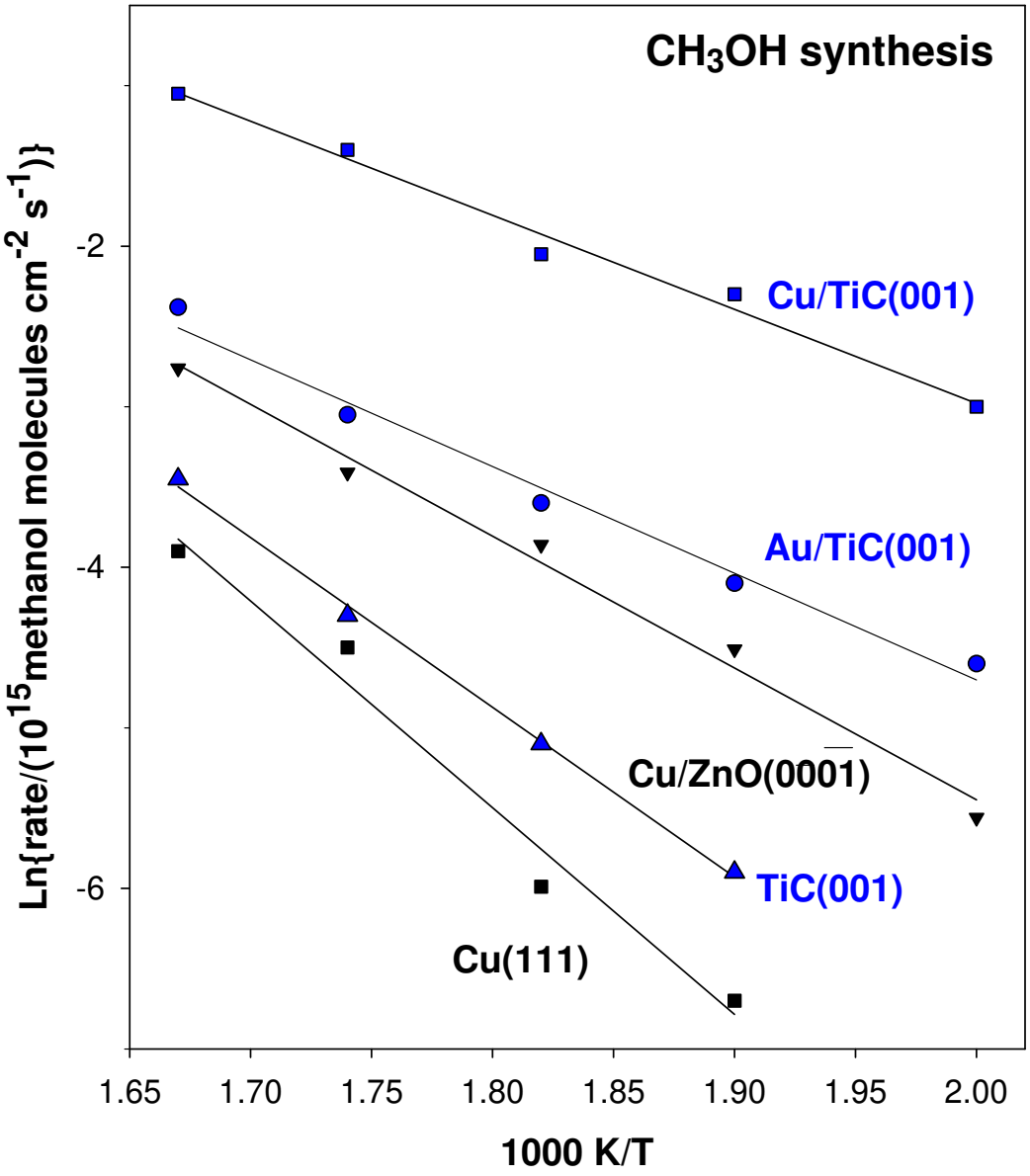
CH3OH synthesis
Cu/TiC(001)
Au/TiC(001)
Cu/ZnO(000$\bar{1}$)
TiC(001)
Cu(111)
Ln{rate/(10^15 methanol molecules cm^-2 s^-1)}
-2
-4
-6
1.65
1.70
1.75
1.80
1.85
1.90
1.95
2.00
1000 K/T

Figure 15

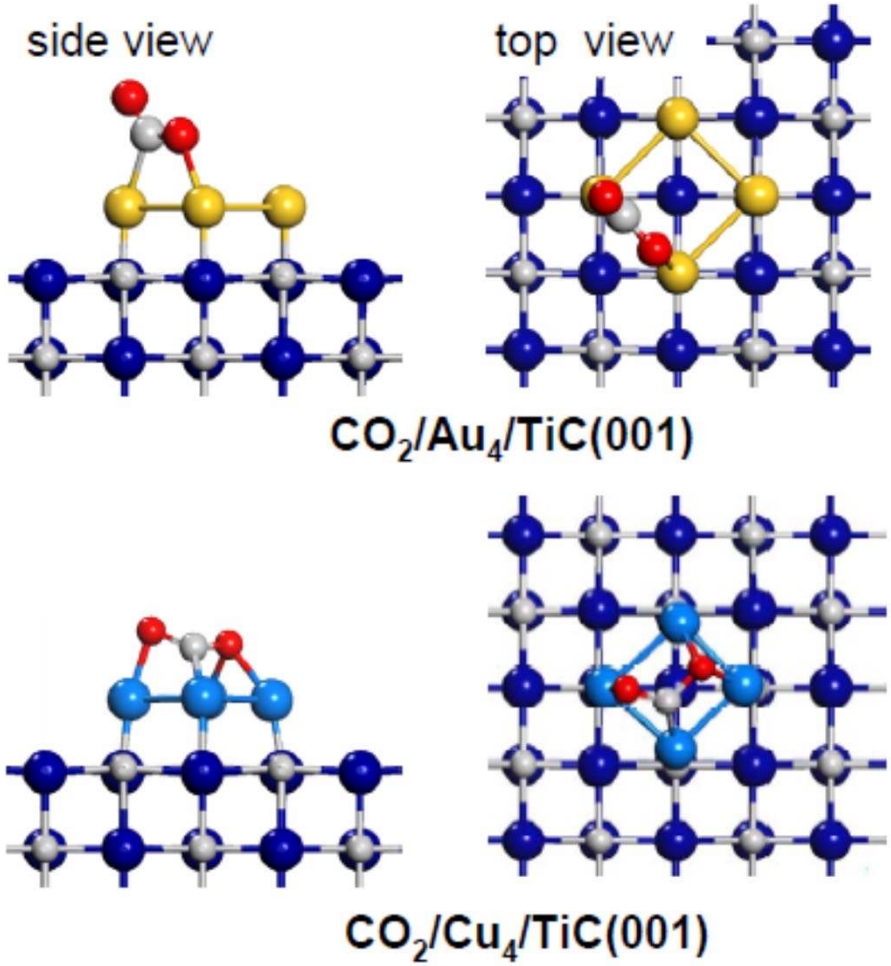
side view
top view
E_{ads}= -0.7 eV
$CO_2/Au_4/TiC(001)$
E_{ads}= -1.1 eV
$CO_2/Cu_4/TiC(001)$

Figure 16

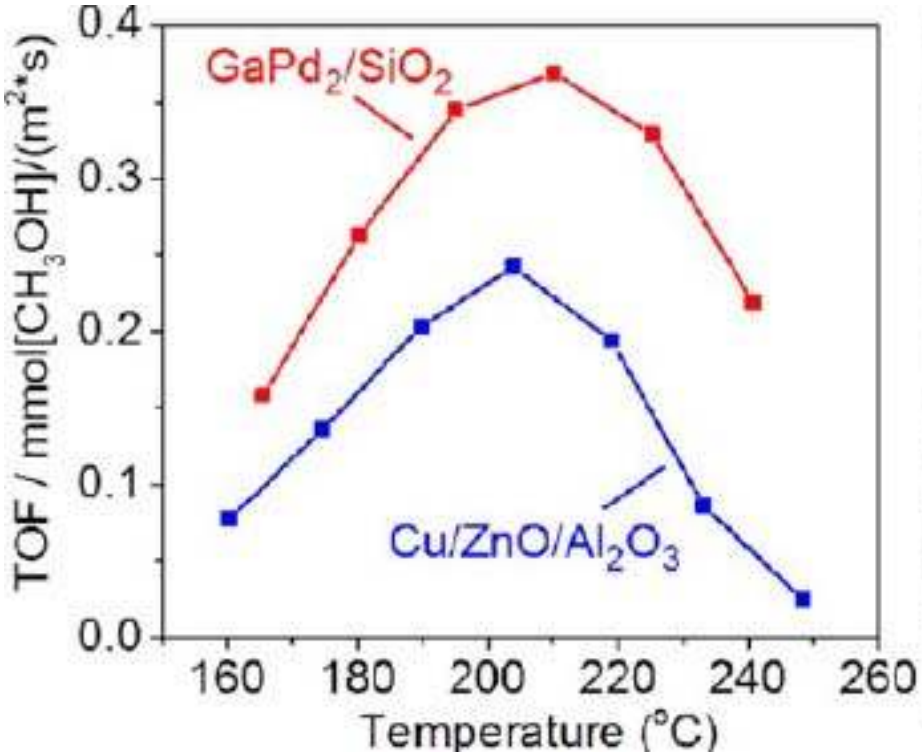
GaPd2/SiO2
Cu/ZnO/Al2O3
TOF / mmol[CH3OH]/(m2*s)
0.0
0.1
0.2
0.3
0.4
160
180
200
220
240
260
Temperature (°C)

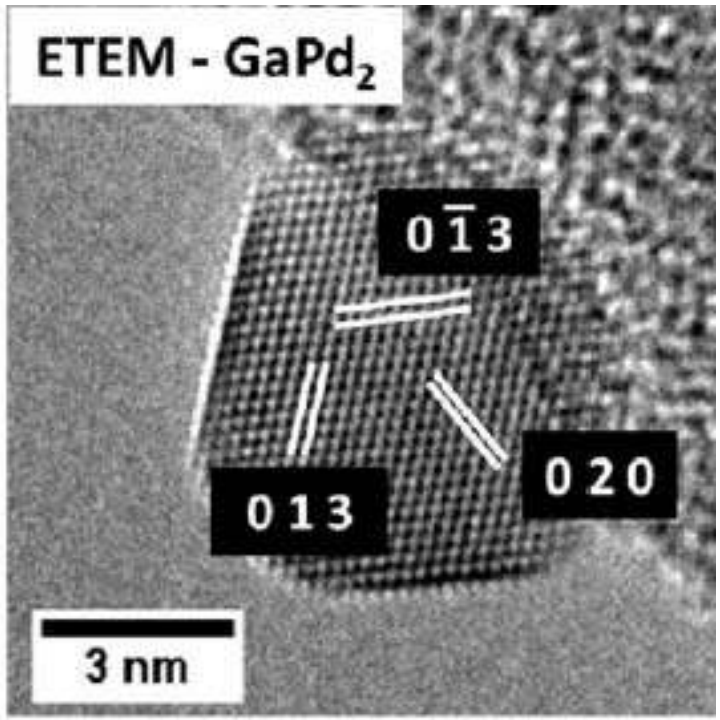
ETEM - GaPd2
0 1̄ 3
0 1 3
0 2 0
3 nm

Figure 17

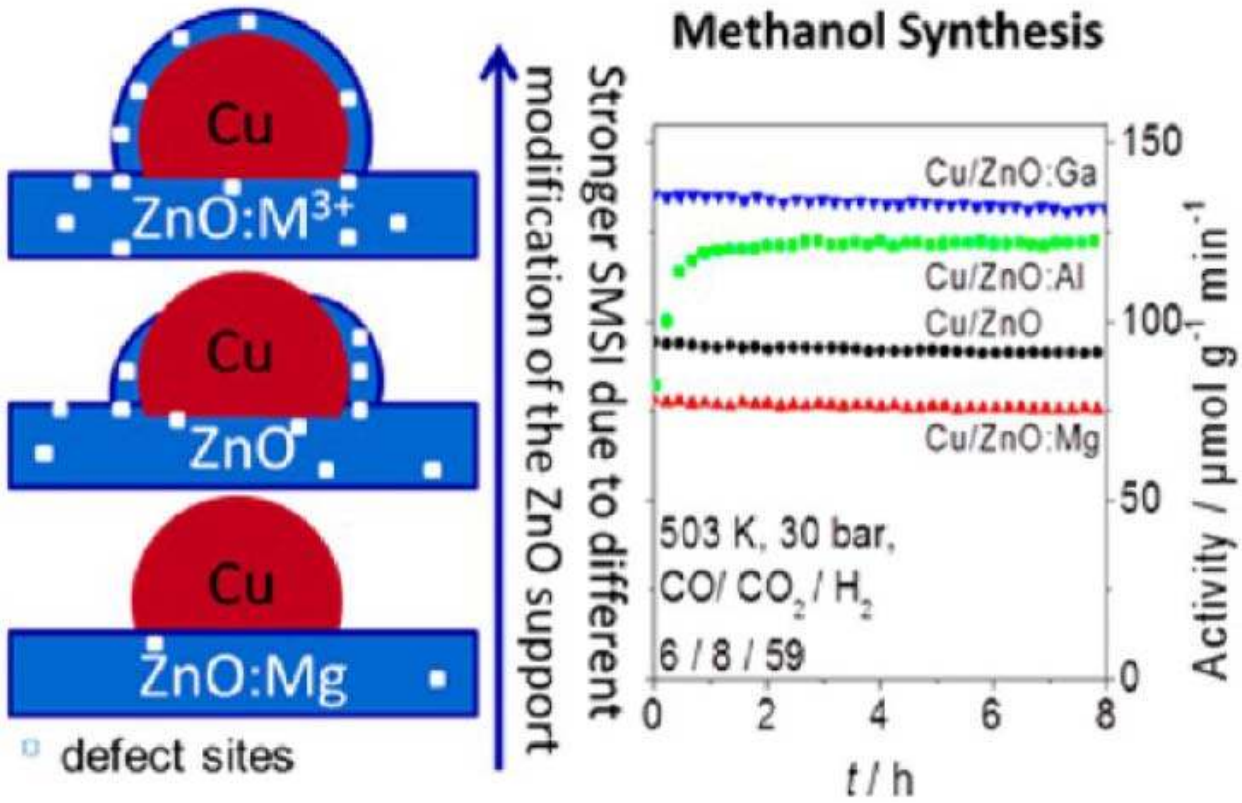
Cu
ZnO:M3+
Cu
ZnO
Cu
ZnO:Mg
defect sites
Stronger SMSI due to different
modification of the ZnO support
Methanol Synthesis
Cu/ZnO:Ga
Cu/ZnO:Al
Cu/ZnO
Cu/ZnO:Mg
503 K, 30 bar,
CO/ CO2 / H2
6 / 8 / 59
0
2
4
6
8
t / h
150
100
50
0
Activity / µmol g-1 min-1

Figure 18

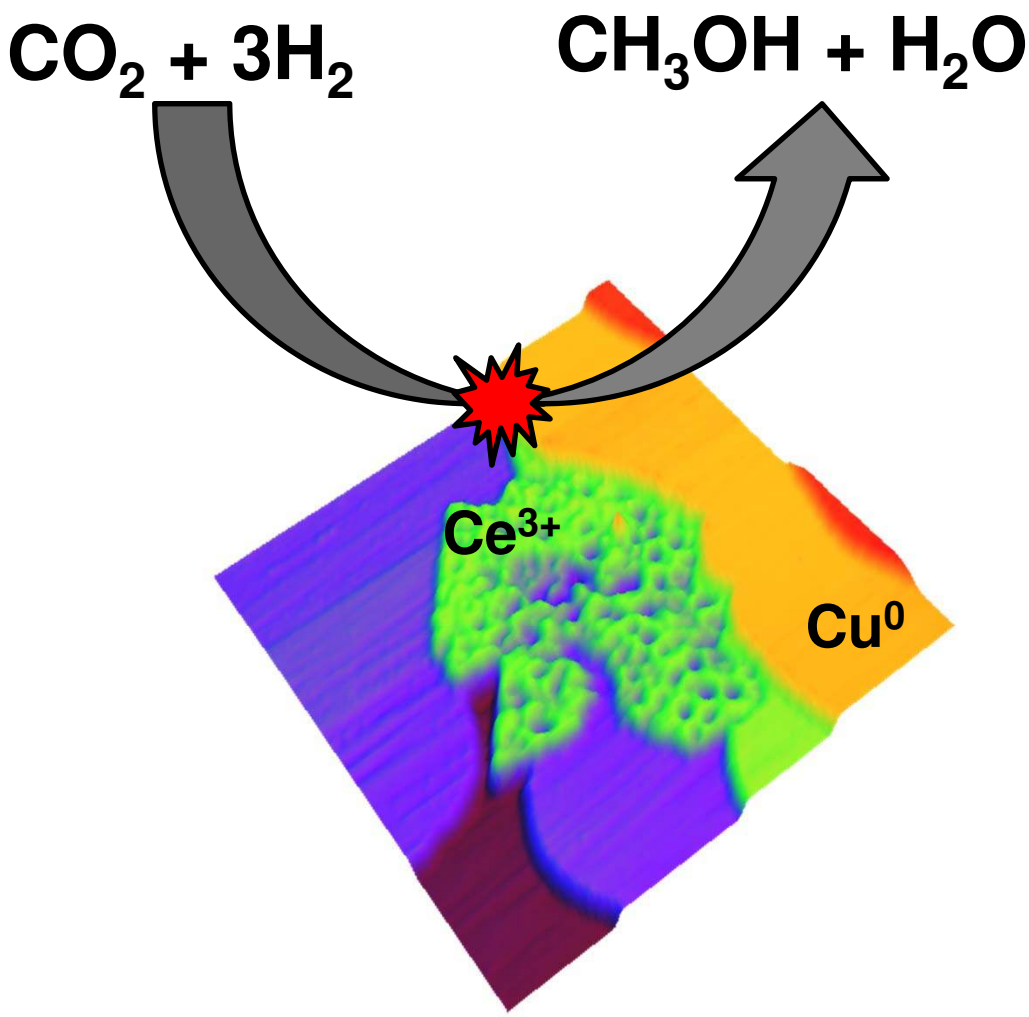

TOC